

**UNIVERSIDADE FEDERAL DE SANTA CATARINA
PROGRAMA DE PÓS-GRADUAÇÃO EM ENGENHARIA
MECÂNICA**

THALES AGOSTINI RIBEIRO BATISTA

**MODELING AND ANALYSIS OF AN ELECTRO-
HYDROSTATIC SYSTEM USING ASYMMETRICAL
CYLINDER FOR INDUSTRIAL AND MOBILE MACHINERY**

Dissertação submetida ao Programa de Pós-graduação em Engenharia Mecânica da Universidade Federal de Santa Catarina para a obtenção do Grau de Mestre em Engenharia Mecânica.

Orientador: Prof. Victor Juliano De Negri, Dr. Eng.

Coorientadora: Tatiana Mivav, Dr.Eng.

Florianópolis, 2018.

Ficha de identificação da obra elaborada pelo autor,
através do Programa de Geração Automática da Biblioteca Universitária da UFSC.

Batista, Thales

Modeling and Analysis of an Electro-hydrostatic
System Using Asymmetrical Cylinder for Industrial
and Mobile Machinery / Thales Batista ;
orientador, Victor Juliano De Negri,
coorientadora, Tatiana Minav, 2019.

119 p.

Dissertação (mestrado) - Universidade Federal de
Santa Catarina, Centro Tecnológico, Programa de Pós
Graduação em Engenharia Mecânica, Florianópolis, 2019.

Inclui referências.

1. Engenharia Mecânica. 2. Electro-hydrostatic
Actuator. 3. Asymmetrical Cylinder. 4. Dynamic
Simulation. 5. Efficiency. I. Juliano De Negri,
Victor . II. Minav, Tatiana. III. Universidade
Federal de Santa Catarina. Programa de Pós-Graduação
em Engenharia Mecânica. IV. Título.

Thales Agostini Ribeiro Batista

**MODELING AND ANALYSIS OF AN ELECTRO
HYDROSTATIC SYSTEM USING ASYMMETRICAL
CYLINDER FOR INDUSTRIAL AND MOBILE MACHINERY**

Esta Dissertação foi julgada adequada para obtenção do Título de “Mestre em Engenharia”, e aprovada em sua forma final pelo Programa de Pós-Graduação em Engenharia Mecânica.

Florianópolis, 12 de abril de 2019.

Prof. Jonny Carlos da Silva, Dr.
Coordenador do Curso

Banca Examinadora:

Prof. Victor Juliano De Negri, Dr.
Orientador
Universidade Federal de Santa Catarina

Prof. Eduardo Yuji Sakurada, Dr.
Instituto Federal de Santa Catarina

Prof. Jonny Carlos da Silva, Dr.
Universidade Federal de Santa Catarina

Este trabalho é dedicado aos meus colegas, amigos e aos meus queridos pais e irmãos.

ACKNOWLEDGMENT

First, I would like to thank my Mom and Dad for all the love and support given to me during my journey, my two little brothers that are also follow their way by my side.

Express my gratitude to my advisor, Prof. Victor Juliano De Negri, for the experience and knowledge shared and his time spent to help and guide me in the right direction. Also my sincere thanks to Dr. Tatiana Minav and Prof. Matti Pietola for the invitation and trust to spend part of my master's period working with their research group.

Thanks to all my colleagues from LASHIP, those who shared the up and down moments during this path, Thiago, Marcos, Rafael, Giuliano, Vinícius, Ivan, Andrei, Nicodemos, Henrique, Túlio, Henri, Job, Diego, Arthur, Nelson, Talles, Gabriel, Gregori, João for the friendship and countless cups of coffee at the lab during the execution of this work.

Thanks to my colleagues from Aalto University, Abinab, Teemu, Han, Tom, Otto, Siavash, Arttu, Heikki, and Olof, for the incredible experience working with the research group.

Tack så mycket till mina kompisar fra Sverige, Cristopher, Daniel, Erik, Viktor Stroberg och Viktor Larsson for lektionerna och vänskapen.

Also to all the amazing people I have met during this period, without them would be so much harder, in special to Andres, Andrea, Barbacoas, Bodega, Carles, David, Vivi, Nano, Fos, Fer, Itzi, Natalia, Ruth, Julio, Javi, Pita, Thomas, Anderson, Isa, Annina, Matteo, Medeia, Emilio, Marco, Mariana, Allyson and Ana, for the unforgettable time in Finland.

Thanks also those friends that were by my side, especially the difficult times, Lucas Arrigoni, Tamara, Ayres, Lucas Bodnar, Thalita, Larissa, Victor, Claudia, Michele and Suzanne.

And finally to POSMEC, for the opportunity of professional and personal growth.

“You don’t have to be great to start, but you have to start to be great.” (Zig Ziglar)

MODELAGEM E ANÁLISE DE UM ATUADOR ELETRO-HIDROSTÁTICO PARA UM CILINDRO ASSIMÉTRICO PARA MÁQUINAS INDUSTRIAIS E MÓBIL

RESUMO

As máquinas de construção e agrícolas possuem um papel importante na indústria moderna. Entretanto, com o aumento dos preços de combustíveis fósseis e da exigência de órgãos governamentais em relação à emissão de gases poluentes, fabricantes e instituições de pesquisa buscam soluções para tornar essas máquinas mais eficientes e menos poluentes. Os sistemas hidráulicos são responsáveis por exercer a força de trabalho das máquinas, por serem sistemas robustos e terem uma grande relação potência/peso. Porém, suas arquiteturas convencionais resultam em uma baixa eficiência energética. Os sistemas convencionais, em sua maioria, são caracterizados pela utilização de válvulas para controle direcional, de vazão e de pressão e sua energia provém do motor de combustão do veículo através de um circuito central. Neste cenário, a utilização de sistemas hidrostáticos, no qual as válvulas são removidas, torna-se uma solução interessante para eliminar perdas de energia por estrangulamento de fluido, mas ainda há a dependência do motor de combustão interna. Um conceito aplicado na indústria de aeronaves, chamado atuador eletro-hidrostático (EHA), tem chamado a atenção por suas características, tais como sendo um sistema compacto, robusto e independente. Nesta solução, cada atuador é acionado por seu próprio sistema e não por um sistema central. Além disso, esta configuração é acionada por um motor elétrico, resultando numa menor emissão de poluentes. Sendo assim, o trabalho desta dissertação está focado na análise do comportamento e eficiência energética de um sistema eletro-hidrostático aplicado em um cilindro assimétrico para elevação de carga. Com o auxílio de MATLAB/Simulink® e uma bancada de testes, foi desenvolvido um modelo matemático adequado para representar o comportamento dinâmico do sistema. Por meio de simulação, foi analisada a eficiência energética durante um ciclo de operação e discutidas possíveis alternativas para viabilizar a utilização do sistema em máquinas reais.

Palavras-chaves: Atuador eletro-hidrostático, Cilindro assimétrico, Simulação dinâmica, Eficiência energética.

RESUMO EXPANDIDO

Introdução

Os sistemas hidráulicos são amplamente utilizados nos mais diversos campos de aplicação. A razão para isto é a sua capacidade de suportar grandes cargas, alta relação força/massa, controle preciso de posição e velocidade, possuem uma auto lubrificação, suportem trabalho com sobrecarga de forma segura e podem ser combinado com outros tipos de sistemas, tais como mecânicos, elétricos ou pneumáticos. (MCCULLOUGH, 2011; LINSINGEN, 2016).

As máquinas de construção e agrícolas possuem um papel importante na indústria moderna, e suas aplicações variam desde a mineração, terminais portuários até colheitas florestais (MINAV, 2011). As máquinas pesadas, classificadas desta forma por utilizarem motores a diesel para fornecer energia, têm chamado a atenção devido às suas baixas eficiências e alta quantidade de emissão de poluentes.

Com os custos cada vez mais altos de extração/produção de combustíveis fósseis e com governos atuando de maneira a reduzir os níveis de contaminação ambiental através de regulamentações, os fabricantes e instituições de pesquisa e desenvolvimento buscam desenvolver sistemas mais eficientes e menos impactantes ao meio ambiente.

Segundo Kagoshima *et al.* (2007, *apud* ZHANG *et al.* 2017b), os sistemas tradicionais, como em uma escavadeira, resultam em uma eficiência energética bastante baixa. O fornecimento de potência é normalmente feito por um motor conectado a uma bomba central e controlada por válvulas direcionais para a movimentação dos atuadores. As válvulas impõem restrições aos escoamentos, provocando perda energia por estrangulamento. Outra desvantagem é a utilização de um reservatório comum, não possibilitando a regeneração de energia.

Uma alternativa para os sistemas tradicionais é a utilização de transmissões hidrostáticas, conforme visto em Costa & Sepehri (2015), em que o sistema central é substituído por sistemas fechados vinculados a cada atuador, sendo que nestes sistemas o movimento do atuador é controlado diretamente pela bomba hidráulica, eliminando as válvulas. Embora esse conceito ainda esteja em fase de experimento, alguns autores já notaram uma melhoria na eficiência energética, como também na redução do consumo de energia.

Nesta dissertação é analisada uma configuração de sistema trazendo um conceito muito empregado na indústria de aeronaves, chamado atuador eletro-hidrostático. Neste sistema é utilizada uma unidade de potência composta apenas por motor elétrico, bomba e cilindro. O sistema foi instalado em um guincho hidráulico e posteriormente testado para comprovar sua funcionalidade. Experimentos foram realizados para analisar comportamento e desempenho durante um ciclo de operação. Com base nos dados experimentais, foi criado um modelo matemático que representa o sistema e depois validado.

Objetivos

O objetivo principal é testar uma configuração de transmissão de potência eletro-hidrostática para um atuador linear assimétrico, utilizando componentes disponíveis no mercado, para aplicação em máquinas móveis ou estacionárias. A funcionalidade é demonstrada por meio de experimentos e simulação, incluindo o estudo da viabilidade do sistema para determinadas aplicação.

Objetiva-se também a validação do modelo de simulação para identificação de aspectos positivos e limitações do sistema visando a continuidade do desenvolvimento do sistema.

Os objetivos específicos consistem em testes experimentais em bancada de teste previamente construída, criação do modelo matemático e análise do sistema.

Metodologia

São utilizados livros e artigos disponíveis para obter informações que sustentam e introduzem o tema a ser dissertado.

Através de um sistema de aquisição de dados adequados e um computador para controle do acionamento, foram obtidos dados experimentais suficientes para auxiliar na validação do modelo matemático construído. Apesar disto, o sistema de aquisição de programa controle utilizado não são parte desta dissertação.

O modelo matemático foi desenvolvido integralmente no software Matlab/Simulink, tanto para simulações como também a geração de figuras e cálculos utilizados para as posteriores análises e discussões.

Resultado e Discussões

O modelo matemático construído foi capaz de representar o comportamento obtido nos testes do sistema. Desta forma o modelo foi considerado válido para calcular e analisar as energias do sistema.

As potências e energias do motor elétrico e do cilindro foram calculadas e então determinadas as eficiências energéticas durante o ciclo. As eficiências foram analisadas e calculadas de duas formas, uma para o movimento de subida da carga e outra para a descida. Para a subida, quem fornece a potência de entrada é o motor elétrico, e a energia disponível no cilindro é o que sai do sistema. Durante a descida, considerou-se que a energia de entrada era a energia potencial disponível no cilindro, e o que chega ao motor é a energia capaz de ser recuperada, assumindo a possibilidade de recuperação de energia.

Por meio da simulação, a operação efetuada na bancada com o sistema levantando uma carga de 40 kg, resultou em uma eficiência energética de 58%. Enquanto na descida o valor de recuperação de energia foi de 46%. Um aumento na carga para 200 kg mantendo a mesmo sinal de entrada de frequência rotacional no sistema, a eficiência energética na subida aumentou para 68% e de recuperação para 64%, mostrando a grande influência da carga principalmente na fase de regeneração. Estes valores foram calculados, considerando apenas a eficiência hidráulica, sem a conversão do motor elétrico.

O motor elétrico e as bombas/motores hidráulicos quando em baixa rotação operam em regiões de baixa eficiência energética. Logo, para avaliar a eficiência energética do sistema, foi simulado em uma condição com frequência rotacional mais alta para que não houvesse tantas perdas principalmente no motor elétrico. Entretanto, notou-se a importância de um bom dimensionamento dos deslocamentos volumétricos em relação razão de áreas do cilindro, e o quanto isso pode limitar certas condições de operação sistema, principalmente na velocidade de atuador. No sistema modelado e validado de acordo com resultados experimentais, a razão de deslocamentos volumétricos 0,7177 é significativamente menor que a razão de área das câmaras do cilindro, 0,75. Em outras palavras, a bomba/motor do lado de menor área é menor do que idealmente poderia ser, sendo uma restrição ao fluido para uma direção de movimento do atuador e insuficiente para suprir fluido na outra direção.

Uma análise foi feita movimentando uma carga de 200 kg e uma rotação do motor elétrico a 600 rpm. Para isso foram calculados níveis de eficiência considerando capacidade de regeneração e sem capacidade

para diferentes razões de deslocamento volumétrico das bombas. Os cálculos resultaram que com uma razão de deslocamento de 0,75, a eficiência com regeneração pode chegar a 67,38% enquanto sem regeneração 42,02%. A razão de deslocamento é fundamental para o bom e eficiente funcionamento do sistema assim como não limitar a faixa de velocidade que o atuador possa operar sem causar uma sobre pressão no sistema.

Conclusão e trabalhos futuros

O modelo matemático foi capaz de modelar o comportamento de um atuador eletro-hidrostático testado experimentalmente. Para a condição testada uma eficiência de 58% e regeneração de 46% foram observadas, porém com um potencial de melhora desses números se operado em condições mais favoráveis do motor elétrico e das bombas/motores no ponto de vista de eficiência.

O sistema foi projetado para ser compacto e fechado para que pudesse ser instalado o mais próximo do atuador, entretanto, algumas vantagens e desvantagens são apontadas.

Como a energia do sistema é elétrica, dependendo de como for provida (por baterias, por exemplo), diminui a dependência do motor a combustão. Isto permite que motores menores sejam instalados diminuindo consumo e emissões. Utilizando energia elétrica, tem-se a vantagem da alta eficiência dos equipamentos elétricos se operados em condições ótimas. Os sistemas de controle direto pelo deslocamento volumétrico tem mostrado ser vantajoso do ponto de vista energético se comparado os sistemas por válvulas. Também possui a capacidade de regeneração de energia.

Porém algumas desvantagens são a dificuldade de dimensionamento das bombas/motores principalmente com atuadores assimétricos, pois as taxas volumétricas de cada câmara devem ser próximas ou iguais aos do deslocamento volumétrico das bombas/motores. Caso contrário, haverá uma resistência ou incapacidade de fornecer vazão necessária, consumindo energia. Outro fator são os vazamentos internos da bombas/motores, principalmente quando o atuador está parado. A posição do atuador não pode ser mantida sem que o motor elétrico esteja em rotação para compensar o vazamento.

Os custos para ter esse tipo de sistemas podem aumentar, devido às trocas e adições de componentes necessários para a nova configuração. Outro fator limitante em maquinários móveis são o espaço

disponível e a adição de peso, pois conversores de frequência e unidade de baterias seriam necessários para fornecer energia.

Por último, por ser um sistema fechado não foi utilizado um sistema de filtragem, o que pode ser necessário após um tempo de utilização para não danificar os componentes devido aos resíduos provenientes de desgaste.

Para trabalhos futuros, sugere-se que sejam feitos experimentos em condições de operação diferentes, por exemplo, em condições de cargas dinâmicas presentes em escavadeiras durante o ciclo de trabalho. Para simular ciclos de trabalhos é necessário um controle de posição para o atuador. Como mencionado anteriormente, a posição é afetada pelo vazamento nas bombas/motores. Para manter posição quando o motor elétrico está parado, pode-se considerar a utilização de válvulas *on-off*. Um estudo do comportamento térmico também é sugerido, pois o sistema não foi submetido testes em longos ciclos de trabalho e uma análise térmica pode apontar a necessidade de um sistema de resfriamento. Por fim, avaliar outras possibilidades de configuração do sistema para tentar diminuir os efeitos negativos da diferença entre as razões de áreas do cilindro e dos deslocamentos volumétricos. Sejam utilizando configurações com uma bomba/motor, bombas/motores com motores independentes, bombas digitais, entre outros.

ABSTRACT

Construction and agricultural machinery play an important role in the modern industry. However, with the increasing of fossil fuel costs and the government's requirements to reduce gas emissions, manufacturers and research institutions are looking for alternatives to make the machines more efficient and less polluting. The hydraulic systems are responsible for transmitting and supplying the energy required by the machine to do its tasks, due to its robustness and the high power density. Still, conventional systems result in low energy efficiency. The conventional systems are characterized by the usage of valves to control the flow direction and the power is provided by an internal combustion engine through a central circuit. In this scenario, the implementation of the hydrostatic system, in which valves are removed, turn in a solution eliminating energy losses by throttling action, but not the combustion engine dependency. A concept applied in the aircraft industry, known as electro-hydrostatic actuator (EHA), got attention for its features, such as robust, compact and independent. In this solution, each actuator is driven by its own system and not sharing a central one. Moreover, this configuration is driven by an electric motor, resulting in fewer emissions. In this manner, this work is focused on the analysis for the behavior and energy efficiency of an electro-hydrostatic system applied in an asymmetrical cylinder to lift the load. With the assistance of MATLAB/Simulink® and a test bench, a mathematical model was developed to represent the dynamic behavior of the system. Through simulation, the energy efficiency was analyzed during an operation cycle and its advantages and disadvantages pointed out, as well as possible alternatives to make feasible the implementation of the system.

Keywords: Electro-hydrostatic actuators, Asymmetrical cylinder, dynamic simulation, Energy efficiency.

LIST OF FIGURES

Figure 1.1- A Simplified hydraulic system in a conventional excavator.	38
Figure 1.2 - Mini excavator hydraulic system using a hydrostatic actuator.	39
Figure 1.3 - Diagram of the electro-hydrostatic actuator system.	40
Figure 1.4 - Stand-alone crane utilized for the system installation.	41
Figure 2.1 - Simplified hydrostatic transmission schematic.....	43
Figure 2.2 - Hydrostatic transmission in the flight control system.	44
Figure 2.3 - Speed-controlled hydraulic system for a ship rudder.	47
Figure 2.4 - Digital pump system.	48
Figure 2.5 - Operating quadrants of the hydraulic actuation unit.....	49
Figure 2.6 - Basic scheme of closed circuit for the symmetric cylinder.	50
Figure 2.7 - Different compensation methods for differential cylinder systems.	52
Figure 2.8 - Examples of EHA in the railway industry: a) EHA for active roll compensation on a train; b) EHA for active yaw damping on a locomotive.	53
Figure 3.1 - Test bench system installed in the crane.....	56
Figure 3.2 - Diagram of the electro-hydrostatic actuator setup.	57
Figure 4.1 - External gear pump/motor schematic. (a) Motor mode and (b) pump mode.	64
Figure 4.2 - Diagram of the pump/motor at the piston side.	66
Figure 4.3 - Diagram of the pump/motor at the piston rod side.	67
Figure 4.4 - Accumulator flows schematic.	70
Figure 4.5 - Hydraulic cylinder schematic.	73
Figure 4.6 - Effects on the motion performance caused by friction forces.	75
Figure 4.7 - Contact between bristles of two surfaces.....	76
Figure 4.8 - Friction map in terms of Stribeck, Coulomb and viscous friction.	77
Figure 4.9 - Friction curve adopted in the simulation.	78
Figure 4.10 - Free body diagram of the crane.	79
Figure 5.1 – Motor rotational speed measured by the encoder.	83
Figure 5.2 - Cylinder position in the performed cycles.	84
Figure 5.3 - Pressure in the piston side volume.....	84
Figure 5.4 - Pressure level in the rod side volume.	85
Figure 5.5 - Pressure level in the accumulator line.	86
Figure 5.6 - Cylinder position simulated and experimental.	87

Figure 5.7 - Piston side pressure simulated and experimental.	87
Figure 5.8 - Rod side pressure simulated and experimental.	88
Figure 5.9 - Pressure in the accumulator line.....	88
Figure 5.10 - Piston side pressure of validation and optimal condition.	89
Figure 5.11 - Rod side pressure of validation and optimal condition . .	89
Figure 5.12 - Pressure in the accumulator line of validation and optimal condition	90
Figure 6.1- Power supplied and consumed during the cycle.....	92
Figure 6.2 - Forces acting in the system along the cycle.	92
Figure 6.3 Efficiency results in the simulation.	95
Figure 6.4 - Energy provided (solid line) and consumed (dashed line) during the cycle considering capacity of regeneration.....	96
Figure 6.5 - Energy provided (solid line) and consumed (dashed line) during the cycle considering no capacity of regeneration.....	96
Figure 6.6 - Simulation curves using 200 kg load compared with 40 kg	98
Figure A.1- Volumetric flow rate pump/motor A	109
Figure A.2 - Mechanical torque pump/motor A.....	109
Figure A.3 - Pressure in the chamber A of the Cylinder.....	109
Figure A.4 - Volumetric flow rate pump/motor B.	110
Figure A.5 - Mechanical torque pump/motor B.....	110
Figure A.6 - Pressure in the chamber B of the cylinder.	110
Figure A.7 - Cylinder friction model.	111
Figure A.8 - End Force.	111
Figure A.9 - Accumulator model.	111
Figure A.10 - Accumulator hose volume.	112
Figure A.11 - Effective bulk modulus.....	112
Figure A.12 - Orifice of the accumulator.....	112
Figure A.13- Check valve flow rate.....	113
Figure B.1 - Curve Flow x Pressure of check valve.....	119

LIST OF TABLES

Table 2.1 - Comparison between different drive concepts.	46
Table 3.1 - List of components in the setup.	58
Table 3.2 - Technical data of the electric motor.	59
Table 3.3 - Main parameters of the external gear motors.	60
Table 3.4 - Main parameters of the linear actuator.	60
Table 4.1 - Typical values for hydraulic fluids properties.	69
Table 4.2 - Friction parameters.	78
Table 6.1 - Influence of volumetric displacement ratio in the hydraulic efficiency and regeneration.	99

LIST OF ABBREVIATION

CVT	Continuously Variable Transmission
DAQ	Data Acquisition Unit
DDH	Direct Driven Hydraulics
EGM	External Gear Motor
EHA	Electro-Hydrostatic Actuator
HT	Hydrostatic Transmission
LASHIP	Laboratório de Sistemas Hidráulicos e Pneumáticos
PBW	Power By Wire
SIMO	Single Input Multiple Output

LIST OF SYMBOLS

*SI*_{Sb}

<i>SI</i>	Literal symbol
<i>Sb</i>	Sub-index

LIST OF SUB-INDEX

<i>0</i>	Initial
<i>1</i>	Fixed segment of the boom
<i>2</i>	Movable segment of the boom
<i>A</i>	A-chamber
<i>Acc</i>	Accumulator
<i>B</i>	B-chamber
<i>C</i>	Coulomb
<i>CV</i>	Check Valve
<i>Cyl</i>	Cylinder
<i>eff</i>	Effective
<i>em</i>	Electric motor
<i>end</i>	Cylinder wall
<i>fluid</i>	Fluid
<i>g</i>	Trapped gas/air in the system
<i>gas</i>	Gas inside the accumulator diaphragm
<i>H</i>	Hose
<i>hm</i>	Mechanical
<i>hyd</i>	Hydraulic
<i>L</i>	Leakage
<i>l</i>	liquid
<i>lift</i>	Lifting motion
<i>load</i>	Load
<i>lower</i>	Lowering motion
<i>m</i>	motor
<i>p</i>	pump
<i>pm</i>	Pump/motor

<i>pro</i>	Provided
<i>S</i>	Stribeck
<i>s</i>	Static
<i>shaft</i>	Pump/motor shaft
<i>total</i>	Total
<i>tr</i>	Transient
<i>turb</i>	Turbulent
<i>v</i>	Volumetric

GREEK ALPHABET

α	Angle between the cylinder and joint	[°]
α_{CV}	Angular coefficient of the check valve	[°]
β	Opening angle of the cylinder with the joint	[°]
β_0	Initial opening angle of the cylinder	[°]
β_{eff}	Bulk modulus of the gas	[Pa]
β_g	Bulk modulus of the gas	[Pa]
β_H	Bulk modulus of the hose	[Pa]
β_l	Bulk modulus of the liquid	[Pa]
γ	Adiabatic constant	[°]
Δp	Pressure difference	[Pa]
Δq	Volumetric flow rate difference	[m ³ /s]
ζ_{end}	Damping coefficient of the end force	[kg/s]
η_{em}	Electric motor efficiency	[-]
η_{hm}	Mechanical efficiency	[-]
η_{lift}	Lifting motion efficiency	[-]
η_{lower}	Lowering motion efficiency	[-]
ρ	Fluid density	[kg/m ³]
Θ	Joint of the crane boom	[-]
θ	Opening angle of the crane boom	[°]
θ_{m1}	Angle between vertical structure and m_1 point	[°]
θ_{m2}	Angle between vertical structure and m_2 point	[°]
θ_{mload}	Angle between vertical structure and m_{load} point	[°]
v	Relative velocity between the two surfaces	[m/s]
ν	Kinematic viscosity	[m ² /s]
σ_0	Stiffness coefficient of the bristles	[N/m ²]
σ_1	Damping coefficient of the bristles	[N.s/m]
σ_2	Viscous friction	[N.s/m]
ω_m	Rotational speed of the motor	[rad/s]
ω_p	Rotational speed of the pump	[rad/s]
ω_{pm}	Rotational speed of the pump/motor	[rad/s]

LATIN ALPHABET

A	Area	[m ²]
A_A	Piston head side area	[m ²]
A_B	Rod side area	[m ²]
A_O	Orifice Area	[m ²]
Cd	Discharge coefficient	[-]
Cd_{turb}	Turbulent discharge coefficient	[-]
d_1	Distance of lowest point of cylinder to the joint	[m]
d_2	Distance of highest point of cylinder to the joint	[m]
D_A	Volumetric displacement of the pump/motor A	[m ³ /rad]
D_B	Volumetric displacement of the pump/motor B	[m ³ /rad]
D_m	Volumetric displacement of the motor	[m ³ /rad]
D_p	Volumetric displacement of the pump	[m ³ /rad]
D_{pm}	Volumetric displacement of the pump/motor	[m ³ /rad]
D_{pmA}	Volumetric displacement of the pump/motor A	[m ³ /rad]
D_{pmB}	Volumetric displacement of the pump/motor B	[m ³ /rad]
E_{Cyl}	Energy in the cylinder	[J]
E_{reg}	Energy regenerated	[J]
E_{req}	Energy required	[J]
F_{Cyl}	Hidraulic force	[N]
F_{end}	End force	[N]
F_{Fr}	Friction force	[N]
J	Moment of Inertia	[kg.m ²]
K_L	Internal leakage coefficient of the cylinder	[m ³ /s/Pa]
K_{LA}	Internal leakage coefficient of the pump/motor A	[m ³ /s/Pa]
K_{LB}	Internal leakage coefficient of the pump/motor B	[m ³ /s/Pa]
K_S	Proportional constant of the hard-stop pressure	[Pa/m ³]
K_V	Volumetric coefficient of the orifice	[m ³ /s/Pa]
k_{end}	Stiffness coefficient of the end force	[kg/s ²]
M_θ	Torque on the joint \ominus	[Nm]
m_1	Mass of the fixed segment of the boom	[kg]
m_2	Mass of the movable segment of the boom	[kg]
p	Pressure	[Pa]

p_A	Pressure in the A-chamber volume	[Pa]
p_{Acc}	Pressure in the accumulator	[Pa]
p_B	Pressure in the B-chamber volume	[Pa]
p_{CP}	Cracking pressure of the check valve spring	[Pa]
P_{Cyl}	Cylinder power	[W]
P_{em}	Electric motor power	[W]
p_{gas}	Pressure of the gas in the accumulator diaphragm	[Pa]
p_{HS}	Hard-stop pressure	[Pa]
P_{hyd}	Hydraulic power	[W]
p_T	Pressure in the reservoir volume	[Pa]
p_{tr}	Transition Pressure	[Pa]
q_V	Volumetric flow rate	[m ³ /s]
q_{VA}	Volumetric flow rate in the A-chamber	[m ³ /s]
q_{VAcc}	Volumetric flow rate in the accumulator	[m ³ /s]
q_{VAT}	Vol. Flow rate in the reservoir line through pump/motor A	[m ³ /s]
q_{VBT}	Vol. Flow rate in the reservoir line through pump/motor B	[m ³ /s]
q_{VB}	Volumetric flow rate in the B-chamber	[m ³ /s]
q_{VL}	Volumetric flow rate of leakage	[m ³ /s]
q_{VLA}	Volumetric flow rate of leakage pump/motor A	[m ³ /s]
q_{VLB}	Volumetric flow rate of leakage pump/motor B	[m ³ /s]
q_{Vo}	Flow rate through the orifice	[m ³ /s]
q_{Vpm}	Flow rate of the pump/motor	[m ³ /s]
R_{tr}	Transition Reynolds number	[-]
r_1	Distance between center of mass m_1 and joint Θ	[m]
r_2	Distance between center of mass m_2 and joint Θ	[m]
r_{load}	Distance between center of mass m_{load} and joint Θ	[m]
S	Cylinder stroke	[m]
T_m	Output torque on the motor shaft	[Nm]
T_p	Input torque on the pump shaft	[Nm]
T_{pro}	Provided torque by the electric motor shaft	[Nm]
T_{req}	Required torque by the electric motor shaft	[Nm]

V_0	Initial Volume of the cylinder chamber	$[\text{m}^3]$
V_{0A}	Initial Volume of the A-chamber	$[\text{m}^3]$
V_{0B}	Initial Volume of the B-chamber	$[\text{m}^3]$
V_A	Volume of the A-chamber	$[\text{m}^3]$
V_{Acc}	Total volume of the accumulator	$[\text{m}^3]$
V_{fluid}	Fluid volume inside the accumulator	$[\text{m}^3]$
V_g	Volume of trapped air in the system	$[\text{m}^3]$
V_{gas}	Volume of gas in the diaphragm	$[\text{m}^3]$
V_{total}	Total volume of the control volume	$[\text{m}^3]$
V_B	Volume of the B-chamber	$[\text{m}^3]$
x	Cylinder position	$[\text{m}]$
\dot{x}	Cylinder velocity	$[\text{m/s}]$

SUMÁRIO

1.	INTRODUCTION	37
1.1	GOALS.....	39
1.2	OUTLINE OF THE THESIS	41
2.	LITERATURE REVIEW	43
2.1	PUMP-CONTROLLED SYSTEMS	43
2.2	DRIVE CONCEPTS	45
2.3	LINEAR ACTUATORS WITH PUMP-CONTROLLED ACTUATION	48
2.3.1	Hydraulic actuation unit operating quadrants	48
2.3.2	Symmetric Cylinder	50
2.3.3	Asymmetric Cylinder	50
2.4	ELECTRO-HYDROSTATIC ACTUATORS	52
3.	TEST BENCH DESCRIPTION	55
3.1	MECHANICAL COMPONENTS.....	58
3.1.1	Electric Motor	58
3.1.2	External gear motors (pump/motors)	59
3.1.3	Hydraulic accumulator	60
3.1.4	Hydraulic cylinder	60
3.1.5	Valves	60
3.2	SENSORS	61
3.2.1	Pressure transmitters	61
3.2.2	Wire incremental encoder	61
3.3	ELECTRIC COMPONENTS	61
3.3.1	Frequency converter	62
3.3.2	Data acquisition card and control system	62
4.	MODELING DESCRIPTION	63
4.1	PUMP/MOTOR MODEL.....	64
4.1.1	Pump/motor flow rate	64
4.1.2	Pump/motor torque	68
4.2	EFFECTIVE BULK MODULUS.....	68
4.3	HYDRAULIC ACCUMULATOR MODEL.....	70
4.4	ORIFICE MODEL	71
4.5	CYLINDER MODEL.....	72
4.5.1	Friction force	74
4.5.2	End force	78
4.6	LOAD	79
4.7	CHECK VALVE MODEL.....	81

5.	VALIDATION OF THE MODEL.....	83
6.	ANALYSIS	91
7.	CONCLUSIONS AND FUTURE WORKS	101
7.1	FUTURE WORKS	102
	BIBLIOGRAPHY	103
	APPENDIX A - MATHEMATICAL MODEL OF THE ELECTRO- HYDROSTATIC ACTUATOR.....	109
	APPENDIX B- CURVE PRESSURE X FLOW OF CHECKVALVE FOR PARAMETER ESTIMATION.....	119

1. INTRODUCTION

Due to the variety of technological requirements, hydraulic systems can be applied in practically all fields of activity, from our day to day activities, such as transportation vehicles and dental equipment until more specific applications as aircraft systems and mobile working machines (LINSINGEN, 2016). The reason for their wide employment is that they have the ability to handle with large loads, high force/torque-to-mass ratio, accurate position and velocity control, and self-lubricating system (which is its own fluid), can operate with overload working safely and also can be combined with mechanical, electrical or pneumatic systems (MCCULLOUGH, 2011; LINSINGEN, 2016). On the other hand, its disadvantages are energy losses associated with fluid flow within tubes/hoses and throttling valves, leakage and some actions to protect the hydraulic components against corrosion and dirt (MINAV, 2011).

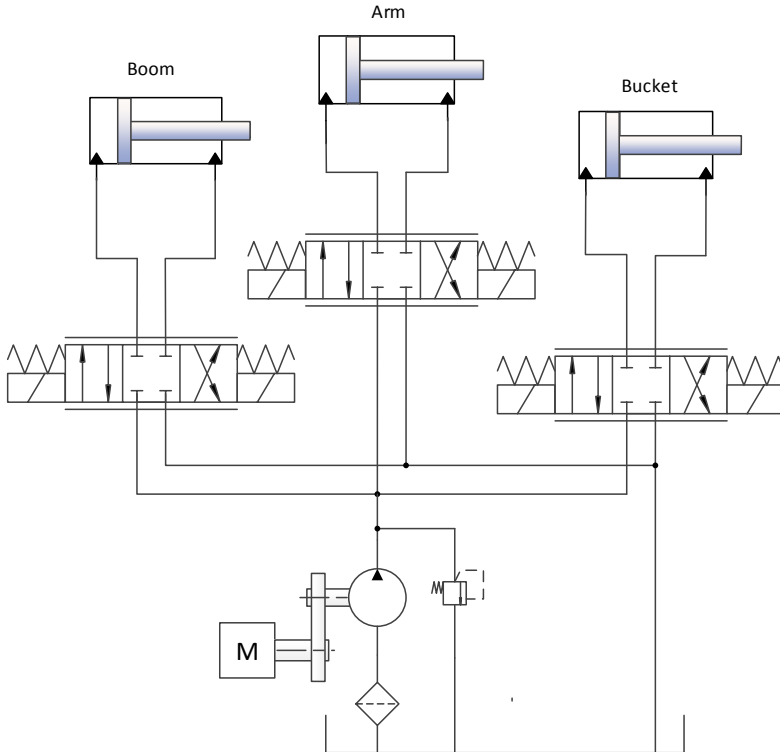
The mobile working machines have an important role in modern industry. They are extensively used for mining, harbor terminal work, forest harvesting, and process manufacturing industry, for example. They can be classified as light mobile machines, when the system works using battery power or heavy mobile machine when its prime mover is a diesel engine (MINAV, 2011). However, the last has got much more attention in these recent years due to its low efficiency and high amount of pollutant emissions.

Considering the increase of oil extraction costs and new governments' carbon dioxide (CO_2), particular matter (PM) and nitrogen oxides (NO_x) emission rules have been implemented for the next years, different system concepts need to be implemented by the industry in order to achieve these regulatory requirements and get higher efficiency.

According to Kagoshima et al. (2007, *apud* ZHANG et al. 2017b), in a conventional excavator the maximum hydraulic power is supplied by a pump coupled to an internal combustion engine and the excessive power is dissipated as heat. It is difficult to reduce input power even during low-workload operation because the actuator control requires a flow distribution. Furthermore, the system operates as an open-circuit, which does not allow energy saving, sending all the potential energy obtained during lift movement back to the reservoir. Figure 1.1 shows a simplified diagram for a conventional excavator where each linear actuator (cylinder) has directional valves to control

flow passage, consequently causing throttling losses and reducing duty cycle efficiency.

Figure 1.1- A Simplified hydraulic system in a conventional excavator.



Source: Author.

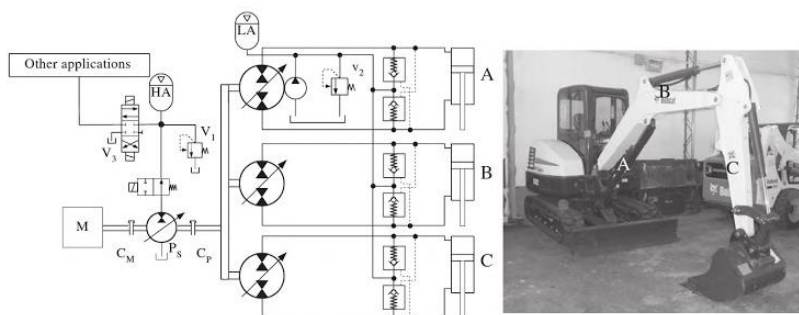
In Costa & Sepehri (2015), the authors stated the possibility, for heavy machines, a replacement of conventional systems by a circuit using a hydrostatic transmission for each cylinder for better control of them, eliminating valves. Nevertheless, several works were published earlier comparing the displacement controlled architecture and the conventional valve controlled. Although that the use of hydrostatic transmission to drive the actuators in heavy machinery is still in experimental phase, some results pointed out that this concept showed an energy saving of 39%, comparing the same machine with load sensing hydraulic system (valve-controlled), and the reduced power

consumption was mainly due to the removing of throttling losses. (WILLIAMSON *et al.*, 2008).

In Hippalgaonkar & Ivantysynova (2013), a displacement controlled mini-excavator was compared with a standard excavator and the results showed a 51% fuel savings without loss of performance, allowing an engine downsizing.

Figure 1.2 shows the hydraulic circuit using a displacement controlled actuator for a mini excavator. This concept revealed to solve the throttling loss problems, but it still depends on the internal combustion engine to run the system. So, in order to improve efficiency, to reduce pollution, and obtain more compact systems, the pump-controlled electro-hydrostatic systems or direct driven hydraulics (DDH) have shown up in recent researches.

Figure 1.2 - Mini excavator hydraulic system using a hydrostatic actuator.



Source: Costa & Sepehri (2015).

1.1 GOALS

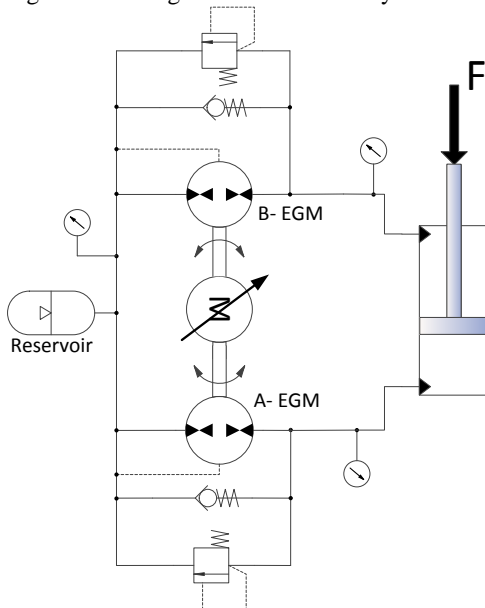
The execution of the present Master's thesis work results from a collaboration between the Laboratory of Hydraulic and Pneumatic Systems (LASHIP) / Federal University of Santa Catarina in Brazil and the Integrated Fluid Power research group of Aalto University in Finland, where part of the work (about 10 months) was carried out. During the period in Finland, experimental tests, system modeling, and thesis and publication writing were done.

This work is focused on a Matlab/Simulink modeling and analysis of an electro-hydrostatic actuator system in performance and energy efficiency point of view. The basic concept of the electro-hydrostatic actuator was previously proposed and installed by the hydraulic research group of Aalto University.

The system is composed of an electric motor, two external gear motors (EGM), a differential cylinder, and one accumulator. The external gear motor utilized is bidirectional due to its constructive parameters, which means that it can operate also as a pump, and along this work it will be also referred as pump/motor. In Figure 1.3 the diagram of the system is shown, where the dimensions of the external gear motor's displacement were defined based on the cylinder dimensions to match as close as possible the flow rates on the cylinder's chambers. A pressurized accumulator was utilized to work as a reservoir in order to provide more compactness to the system and discarding the need for an opened reservoir. Check valves and pressure relief valves were employed in the circuit to avoid cavitation and peaks of pressure when the actuator reaches its end of the stroke.

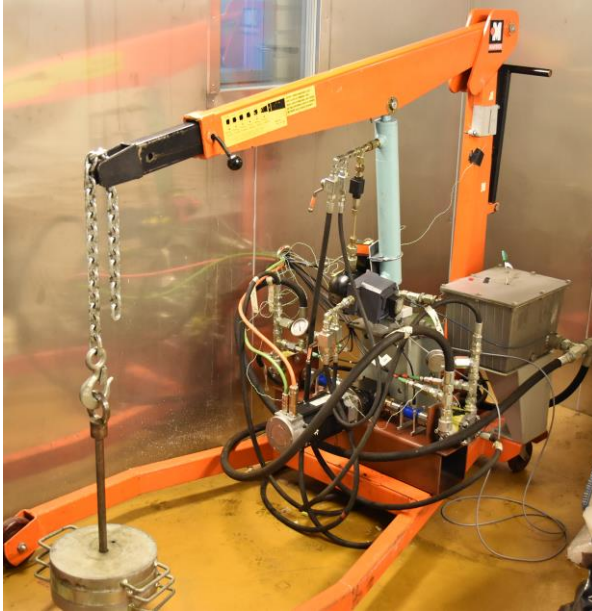
The system was installed in a stand-alone crane shown in Figure 1.4 and utilized to measure and analyze the system behavior to validate the model created. The goal of this work is to evaluate the availability and advantages of this system configuration, in terms of energy efficiency, in low power cranes and mobile machinery.

Figure 1.3 - Diagram of the electro-hydrostatic actuator system.



Source: Author.

Figure 1.4 - Stand-alone crane utilized for the system installation.



Source: Järf (2016).

1.2 OUTLINE OF THE THESIS

The manuscript is organized as follows:

- Section 2 presents a literature review describing the concepts of pump controlled systems and introduces the electro-hydrostatic actuator technology;
- Section 3; characterizes the setup and its components employed to validate the model;
- Section 4 describes the mathematical model utilized to build the model in Matlab/Simulink
- Section 5 presents the validation of the model;
- Section 6 shows the results obtained and analyzes of measurement and simulation;
- Section 7 the conclusions and suggestion for future work

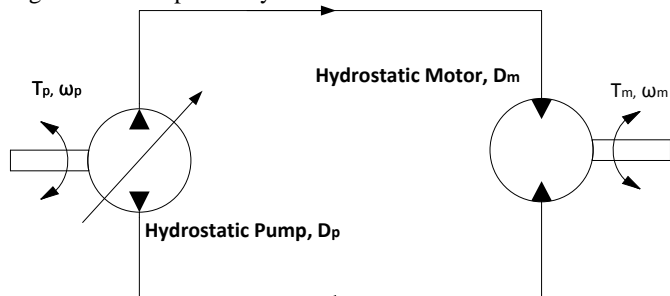
2. LITERATURE REVIEW

In order to model and analyze the behavior of electro-hydrostatic systems, it is first necessary to understand the theory underlying of pump-controlled systems, drive concepts, types of actuators utilized and electro-hydrostatic actuators.

2.1 PUMP-CONTROLLED SYSTEMS

The increasing demand for more efficient systems and for reducing energy costs have led the industry to seek new solutions to replace the traditional hydraulic control systems. These systems have relied on throttle valves, such as proportional valves, servo valves, and flow control valves, and have been shown to have a consumption of 35% for the input energy in controlling valves, leading to a higher engine installed power and consequently higher fuel consumption (QUAN *et al.*, 2014). One method to overcome this problem is to implement a direct pump-controlled system. This method controls the pressure/flow of the hydraulic system through actuation of the pump or the primary power source (e.g., an electric motor or internal combustion engine). An example of a pump-controlled system is shown in Figure 2.1. The system represents a simplified hydrostatic transmission (HT) which is composed of a variable displacement hydrostatic pump driving a fixed displacement hydrostatic motor. The volumetric displacement for the pump is represented by D_p and for the motor by D_m , the rotational speed of the pump and motor are shown by ω_p and ω_m , respectively, and T_p is the torque on the pump shaft and T_m the torque on the motor shaft.

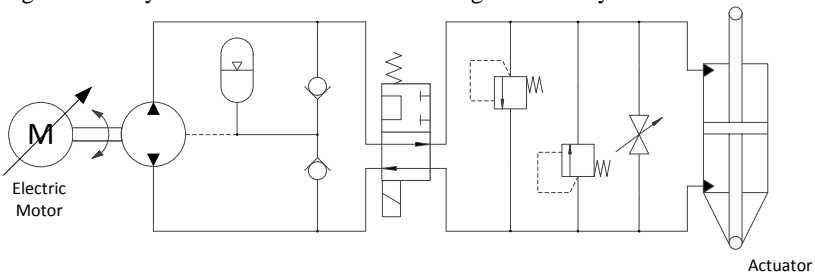
Figure 2.1 - Simplified hydrostatic transmission schematic.



Source: Adapted from Manring (2016).

These transmission systems have been widely applied as it offers a continuously variable transmission (CVT) that aids power transfer without utilizing a discrete number of gear ratios. CVTs are generally used for propelling off-road vehicles, such as construction, earth moving, lawn and gardening machines, but also have become mostly utilized in on-road vehicles allowing the internal combustion engine to operate at its most efficient operating point for a given power requirement (MANRING, 2016). In addition, pump-controlled systems have become well established in the aeronautic industry for various flight control systems, including flaps, ailerons, elevators, and rudders. Figure 2.2 presents the closed circuit utilized in aircraft. The accumulator is used as a filling circuit to avoid a decrease in pressure during system operation caused by internal leakages in the pump or valves.

Figure 2.2 - Hydrostatic transmission in the flight control system.



Source: Adapted from Zhang *et al.* (2017a).

In both examples, the actuators are symmetric (rotary and linear), which results in a flow balance between in and outflows and consequently in considerable simplifications of the system (HABIBI & GOLDENBERG, 2000). However, symmetrical actuators are commonly less preferred than asymmetrical actuators due to the requirements of the installation space and output force. This leads to a different volume flow rates in the two ports of the actuator. In closed-loop systems (i.e., hydrostatic transmission), if the differential flow cannot be compensated, it will affect the accuracy of the piston position, control performance, and energy efficiency (QUAN *et al.*, 2014). Asymmetrical cylinders are mostly utilized in construction machines. The conventional system employed in the machines consists of valves controlling the flow to the actuators, resulting in low-efficiency work during the duty cycle. Pump-controlled systems have been applied in construction machines at

the Fluid Power Research Center at Purdue University since 1998, resulting in circuit simplifications, weight reduction, improvement of energy efficiency, and easier control (QUAN *et al.*, 2014).

Hereafter, several studies have applied pump-controlled actuation for power transmission in construction, agriculture, and mining machines. For example, Williamson *et al.* (2008) compared the energy consumption of a pump-controlled excavator and a valve-controlled excavator, showing that the pump-controlled excavator consumed 39% less energy than the valve-controlled.

2.2 DRIVE CONCEPTS

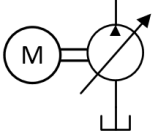
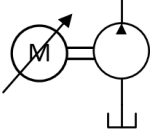
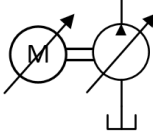
Pump control can be adjusted using two different approaches: Direct and indirect control. Direct control can be achieved by changing the displacement of the pump, which changes internal parts of the variable-displacement pump (e.g., swash plate axial piston pump). On the other hand, indirect control can be indirectly achieved by changing the rotational speed of the pump; in this case, both variable-displacement pumps and fixed-displacement pumps (e.g., external gear pump) could be utilized.

According to Tašner *et al.* (2014), in most machines are implemented the direct concept. Still in recent years, the usage of the variable-speed motor with a constant-displacement pump concept has become more popular due to the desire for greater robustness, and the price decreasing of electrohydraulic drives and motor controllers. However, the indirect concept cannot meet the dynamic requirements of the direct concept. In Lovrec & Ulaga (2007) is presented as an experimental test for both concepts, where the variable-displacement pump controlled system had a response four to five times faster than the fixed-displacement pump controlled system. Considering most of hydraulic applications the responses of both concepts are acceptable.

According to Tašner & Lovrec (2011, *apud* Tašner *et al.*, 2014), another configuration for the pump-controlled system has appeared lately, but the concept is still not very exploited in the industry. It consists of a variable-displacement pump and a variable speed prime mover. Such a concept is difficult to control due to the need of a bivariable controller known as SIMO (Single Input Multiple Output), which two variables are changed, rotational speed and displacement, to affect the pressure.

Table 2.1 presents a comparison between the three different configurations cited previously.

Table 2.1 - Comparison between different drive concepts.

	Direct Approach -Asynchronous Motor -Variable Axial Piston Pump	Indirect Approach -Variable Frequency -Drive Controller -Asynchronous Motor -Constant Gear Pump	Displacement and Speed Variable -Variable Frequency Drive Controller -Asynchronous Motor -Variable Axial Piston Pump
Scheme			
Efficiency	Lower	Higher	Highest
System Dynamics	Highest	Low	Control Principle Dependent

Source: Adapted from Tašner *et al.* (2014).

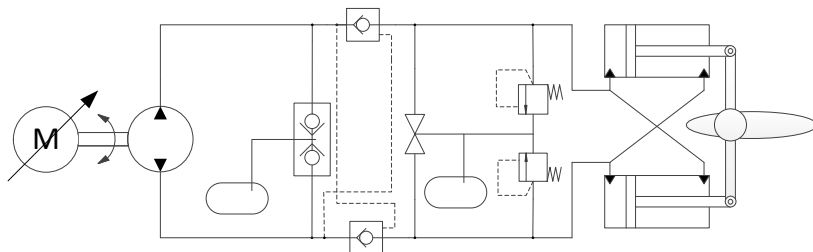
Despite the indirect approach has a slower response and poor low-speed behavior comparing to the direct approach, it is a promising drive principle due to its higher energy efficiency and wide speed range. (XU *et al.*, 2013). The concept of utilizing the variable-displacement pump and variable speed motor seems the best option, but prices are still high.

In addition, Helduser (1999) compared the energy consumption of a displacement-controlled drive and a speed-controlled drive in a specified duty cycle for one hour. The tests showed a reduction of 22.43% of the energy consumption for the speed-controlled drive, which hardly can be achieved by improving the component efficiency.

Due to these advantages, speed-controlled systems have found a wide range of application, been applied in forging machine, injection molding machines, and other machines (HABIBI & GOLDENBER, 1999; HELBIG, 2002; DAHMANN, 2002, *apud* JIANG *et al.* 2004).

In Jiang *et al.* (2004) an example where a conventional ship rudder system is replaced by a speed-controlled hydraulic system is shown. It consists of an AC servo motor driving a bidirectional fixed displacement pump controlling the cylinders directly, as shown in Figure 2.3.

Figure 2.3 - Speed-controlled hydraulic system for a ship rudder.



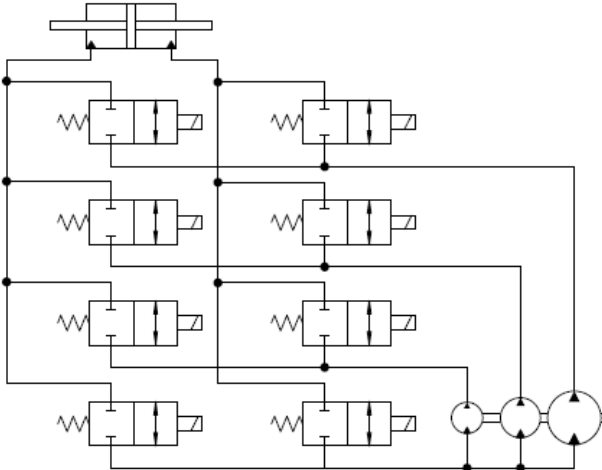
Source: Adapted from Jiang *et al.* (2004).

Through a push-pull mechanism, it converts the hydraulic power to mechanical power to change the position of the ship rudder. The shuttle valves connected to a pressurized reservoir are utilized to compensate oil leakage. Two pilot-operated check valves are installed in series in the closed-loop working as a lock valve; it prevents the flow returning caused by the wave forces acting in the ship rudder.

Besides the improvement of efficiency in the system operation found in their research, it has other advantages such as reduction of the space in almost 1/8 of the original, and reduction of the mass in 50%. With this the implementation of it has created good expectations.

Another alternative of drive concept for energy savings are the digital pumps. The digital pumps consist of several fixed displacement pumps with different sizes rotating in a common shaft. These pumps work in parallel, and through a combination of several switching on-off valves the individual flows are combined and resulting the flow that drives the actuator (HEITZIG & THEISSEN, 2011). Another configuration of digital pumps is to use piston pumps, which each stroke can be independently controlled, allowing pump, motor or idle mode as well as partial strokes (LINJAMA, 2011). Presented by Linjama *et al.* (2009, *apud* Belan *et al.*, 2016), this concept has led to several studies in most areas of application. In Belan *et al.* (2015) an implementation of the digital pumps for a multi-chamber differential cylinder for aircraft. Figure 2.4 shows a schematic of a digital pump system.

Figure 2.4 - Digital pump system.



Author: Heitzig & Theissen (2011).

2.3 LINEAR ACTUATORS WITH PUMP-CONTROLLED ACTUATION

Hydraulic actuators are responsible for converting hydraulic power into useful mechanical power. The actuators can be classified according to motion type they perform, such as continuous rotary (hydraulic motors); limited angular displacement (hydraulic rotary actuators); and linear (hydraulic cylinders) (RABIE, 2009).

The hydraulic cylinders are the most utilized type of hydraulic actuators in hydraulic systems. In relation to the operating principle, they are divided in single-acting and double-acting and considering the area in both chambers, they are classified as symmetrical or asymmetrical cylinders. (TOTTEN & DE NEGRI, 2011, Ch.1).

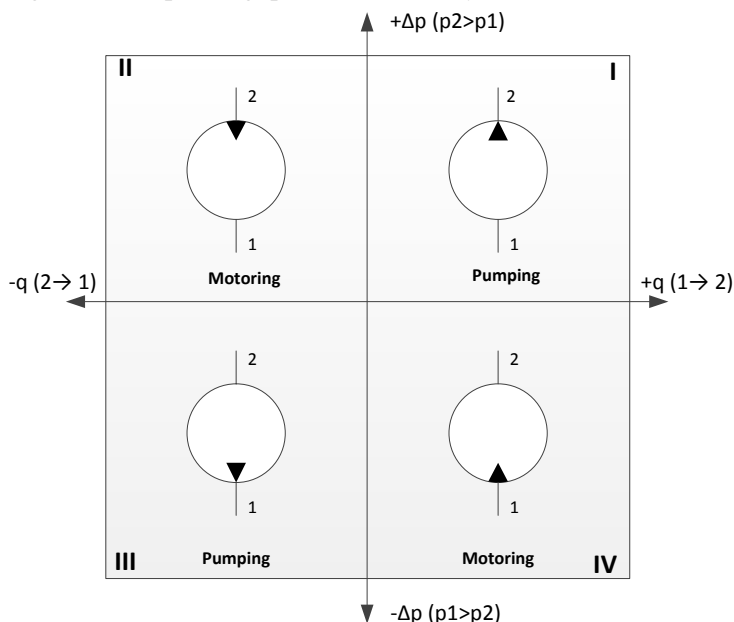
Before presenting the characteristics of the linear actuators, it is important to introduce the hydraulic power unit utilized through its operation modes.

2.3.1 Hydraulic actuation unit operating quadrants

An important device to consider when designing the hydraulic system is the hydraulic conversion unit, utilized to convert mechanical energy into hydraulic energy and vice versa. This unit can be a pump or

a motor, unidirectional or bidirectional depending on its working principle and construction. One method to illustrate the operation mode of a hydraulic conversion unit is making use of the operation quadrants diagram shown in Figure 2.5 (KOMSTA, 2013, *apud* TEIXEIRA, 2015).

Figure 2.5 - Operating quadrants of the hydraulic actuation unit.



Source: Author based on Teixeira (2015).

The diagram presents the horizontal axis which is related to the volumetric flow rate direction through the unit and the vertical axis which considers the pressure difference between the input and output ports. When the flow signal has the same as the pressure difference, the unit operates in pump mode seen in quadrants I and III, which means it is adding hydraulic power in the hydraulic system, converting mechanical energy into hydraulic. Differently, when the signals of the volumetric flow rate and pressure difference are not the same, quadrants II and IV, the unit is taking energy out from the hydraulic system, in other words, it is working in motor mode region, converting hydraulic energy in mechanical. In this case, the unit should be coupled to a component or system able to dissipate, store or transfer energy from the

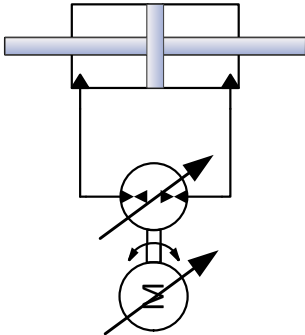
hydraulic system, such as generator. Depending on its constructive principles, a unit converter can operate in both modes of operation.

2.3.2 Symmetric Cylinder

The symmetric cylinder has the same area on both chambers. This leads to a balance between inlet and outlet flow rates of fluid in the cylinder and, consequently, an equal velocity and hydraulic force during extension and retraction actions.

When utilizing symmetric cylinders, the system designing is relatively simple (see Figure 2.6), meaning that there is no need the addition of an auxiliary system in order to compensate fluid in any of those sides in an ideal condition. In case of leakage in the drain line a pressurized reservoir is necessary.

Figure 2.6 - Basic scheme of closed circuit for the symmetric cylinder.



Source: Author.

2.3.3 Asymmetric Cylinder

The asymmetrical cylinder (or differential) can consist of a single or double rod with different sectional areas of the chambers. It results in an unbalanced volume flow rate in the two ports. If operated in a closed circuit, the asymmetrical flow rate needs to be compensated somehow to avoid problems related to the cylinder positioning and control performance, affecting the energy efficiency.

In Destro (2014) and Destro & De Negri (2018), the interaction and behavior of the hydraulic technology and electric devices and components for electro-hydraulic positioning systems is analyzed. In his work the challenges of the valve and actuator selection in order to meet

static and dynamic specifications in positioning systems, based on pressure analysis under different load effects, is evaluated. Both symmetrical and asymmetrical cylinders were studied with proportional valves controlling inlet and outlet flows, and discussed the influence in the pressures of the relation between area ratio of the chambers and the valve flow coefficient ratio, as well as the direction of the load.

In case of electro-hydrostatic systems, which the positioning system is controlled by pumps, the selection of components and the correct configuration are essential to avoid critical conditions, such as overpressure.

According to Quan *et al.* (2014), differential cylinders are mostly employed in electro-hydraulic systems, around 80%, due to the requirements on space-saving and output force. For this reason, researches have studied different methods to compensate the asymmetric flow in differential cylinder system along with its improvement on energy efficiency. Figure 2.7 presents existing methods for compensation utilizing pump-controlled differential actuator system.

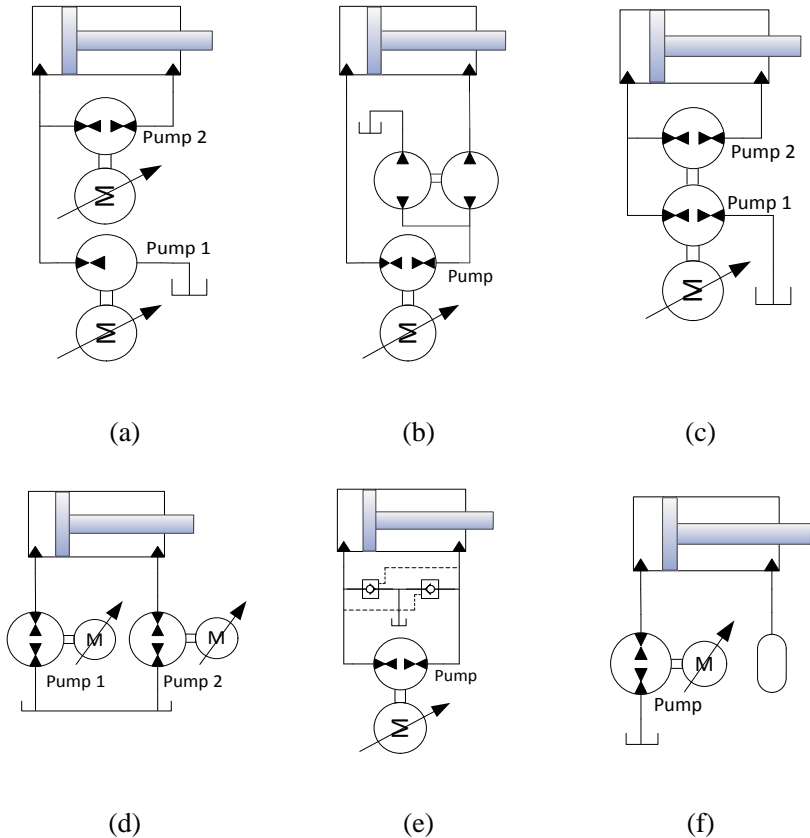
Figure 2.7(a) and (c) utilizes the same concept to compensate the missing fluid necessary in the piston head chamber, adding a pump/motor in the system. When advancing the actuator, the pump/motors referred to pump 1 in the drawings provide the difference of volumetric flow rate in the chamber and the fluid provided by pump/motor 2. The same way, when the cylinder is retrieving the pump 1 operates as a motor and sends the excess of fluid back to the reservoir.

The method proposed in Figure 2.7(b) utilizes two pump/motors to divide volumetric flow rate from the main pump, sending just the required flow to the piston rod chamber and the remaining the other pump in parallel send to the reservoir.

Figure 2.7(d) shows another method where each chamber is connected to a single pump/motor and the units operate synchronized to match the same inflow and outflow.

Other options also can be considered, connecting piloted check-valves to balance the asymmetric flow rates, presented in Figure 2.7(e), but it will increase the energy consumption of the system. A different approach utilizing a pressurized accumulator to retrieve oil, as presented in Figure 2.7(f), where the actuator is working similarly as a single effect actuator.

Figure 2.7 - Different compensation methods for differential cylinder systems.



Author: Adapted from Quan *et al.* (2014).

2.4 ELECTRO-HYDROSTATIC ACTUATORS

The principle of the electro-hydrostatic actuator (EHA) is to convert electric energy into mechanical within one unit. EHAs are typically composed of electric motor, which provides rotational motion to the hydraulic pump (or motor) directly connected, and the hydraulic pump supply hydraulic power to the hydraulic actuator (linear or rotary) (GAILE *et al.*, 2016).

EHA is a power by wire (PBW) technology utilized to replace the traditional centralized hydraulic system by separated power units developed for civil aircraft from 1990s and still are under development.

It means that instead of installing a centralized circuit and power lines through the aircraft, it uses electric signal wires to drive the actuators (ALLE *et al.*, 2016).

Reducing the number of pipelines and joints can overcome several disadvantages of centralized systems such as leakages and pressure drops. It also helps in to simplify the aircraft layout and reducing weight. In large aircraft it is expected 75% of the mass for the hydraulic system is for a power distribution network and only 25% is for pumps and actuators (Maré, 2017).

Besides aircraft applications, EHAs have succeeded in different areas, for instance in the railway industry, reducing significantly the hydraulic system (up to 70%). In case of failure, the replacement of the system becomes faster and the train can be put in operating more quickly. Typical applications are active roll compensation, active lateral suspension and active yaw damping (GAILE *et al.*, 2016) (see Figure 2.8).

Figure 2.8 - Examples of EHA in the railway industry: a) EHA for active roll compensation on a train; b) EHA for active yaw damping on a locomotive.



a)



b)

Source: Gaile *et al.* (2016).

Therefore, the concept of EHA has been considered as an option especially in the mobile machine industry. The decentralized, compact, robust, and more energy efficient unit could lead to a reduction of pollutant emissions and fossil fuel dependence.

The mobile industry plays an important role in the fluid power community. Several researches have been focused on reducing energy consumption and energy efficiency by improving the circuit designs and changing valve-controlled to displacement-controlled concept. However, the implementation of electric motors as a prime mover in this field still has potential to be studied.

Michel & Weber (2012) presented two system architectures for an electrohydraulic compact drive for asymmetric actuators based on the EHA concept. For low applications (less than 5 kW), the level of efficiency reached in his experiments was about 52.8 to 62.3%. Optimizing the component sizes, the efficiency of the electrohydraulic system almost corresponded to the efficiency of an electromechanical drive with a ball screw, around 72.3%. Besides the efficiency, its advantages are robustness and impact absorption. However, the costs also increase compared to the hydromechanical actuator, which must be considered for EHA's implementation. Other factor that is important to consider is the necessity of the frequency converter to control the electric motor. Frequency converters are reliable due to its standard and quality control required. However, depending on the case the converter it can be heavy and requires a lot of space, which can be challenging for a mobile application due to the limited space. It also introduces electrical noise which is undesirable.

3. TEST BENCH DESCRIPTION

In this chapter a detailed description of both hydraulic and electrical components of the electro-hydrostatic actuator system and the working principle is given for a better understanding. This system configuration was proposed previously by Zhang *et al* (2017b) in order to update the system presented in Järf (2016). The main system was constructed and installed (hydraulic and electric components) by the research group in Aalto (see Figure 3.1). During the execution of the thesis, the experimental tests were carried out by the author with the system previously installed. However, it was suggested an addition of some components (relief valves and check valves) mainly for safety and to prevent issues that will be mentioned later. The modified system is presented below and the experimental test was used for this work.

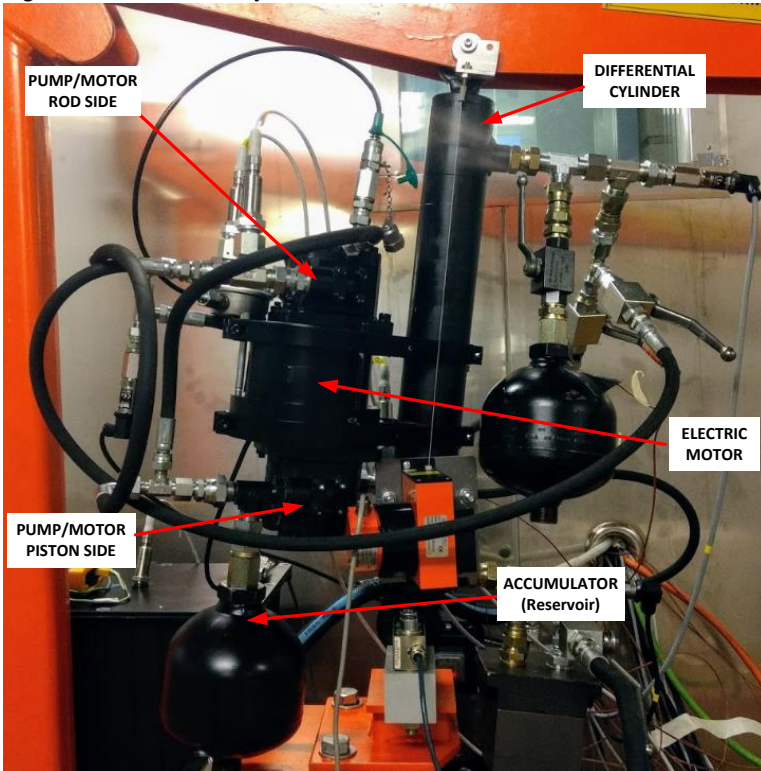
The setup consists of an independent hydraulic circuit installed in a mobile boom crane platform shown in Figure 3.2. The angular position of the boom is controlled by a differential cylinder. The cylinder drives the crane up and down according to the inflow and outflow of the cylinder, provided by two external gear motors. One of these is connected to the piston head side chamber (from now it will be also called A-side) and the other to the piston rod side chamber (B-side). When lifting, pump/motor A (2) is utilized to supply hydraulic power while the other pump/motor B (3) works at the opposite direction taking flow out of the chamber, which means that works as a hydraulic motor. When lowering, the pump/motors will change their function. The other sides of the external gear motors are connected to a common line to a hydraulic accumulator; this component is responsible for supplying hydraulic fluid or store the flow difference between both pump/motors, acting as a reservoir.

Both pump/motors are connected to an axis of a common electric motor which controls the rotational frequency of the pump/motors. In other words, the hydraulic flow rates are directly controlled by the rotational speed of the electric motor. The load utilized in the experiments are composed of plate weights of 20 kg each attached by a chain at the end of the boom.

For reasons of safety and protection especially for the pump/motor against cavitation, pressure relief valves and check valves are installed connecting the cylinder chamber lines to the reservoir line. In case of pressure decrease, the check valve will allow fluid from the

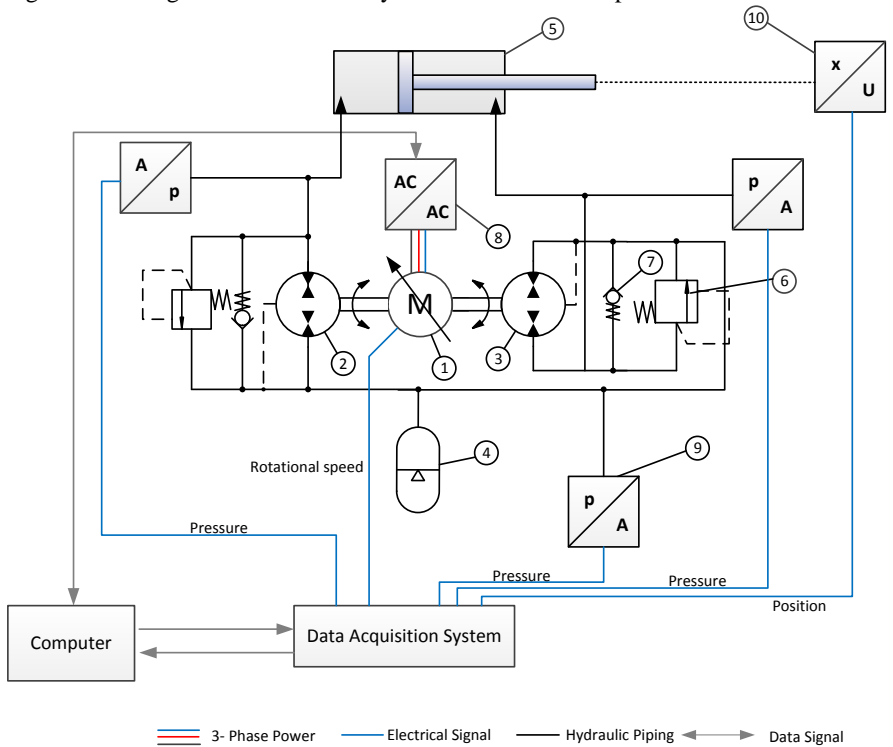
reservoir to the actuator line, and the relief valves will open when the actuator reaches either the end positions.

Figure 3.1 - Test bench system installed in the crane.



Source: Author.

Figure 3.2 - Diagram of the electro-hydrostatic actuator setup.



Source: Author.

Table 3.1 shows the list of components with a reference to the numbers presented in Figure 3.2. The following sections will describe each component in more detail.

Table 3.1 - List of components in the setup.

Number	Component
1	Electric Motor
2	Piston Head Side Pump/Motor
3	Piston Rod Side Pump/Motor
4	Hydraulic Accumulator
5	Differential Cylinder
6	Relief Valves
7	Check Valves
8	Frequency Converter
9	Pressure Sensor
10	Position Sensor

3.1 MECHANICAL COMPONENTS

This section presents each mechanical and hydraulic component selected to build the setup. They consist of an electric motor, external gear motors (or pump/motors), accumulator, valves, and cylinder.

3.1.1 Electric Motor

The prime mover utilized to deliver power to the external gear motors is a Rexroth IndraDyn T Synchronous Torque motor. The motor consists of a stator and a rotor and has a high torque with an optimum residual ripple. This type of motor is very suitable for compact direct drives, according to the manufacturer. The technical data of the selected motor is presented in Table 3.2.

Table 3.2 - Technical data of the electric motor.

Motor Data	Unit	Size 130A-0250
Rated torque	Nm	4.5
Rated power	kW	1.2
Rated current	A	3.5
Rated speed	rpm	2500
Maximum torque	Nm	13
Maximum speed	rpm	4000
Mass of the stator	kg	2.4
Mass of the rotor	kg	0.65

Source: Rexroth IndraDyn T catalog.

3.1.2 External gear motors (pump/motors)

In this system, the conversion of mechanical energy to hydraulic is made by two external gear motors. The external gear principle was considered especially for its robustness and relatively low-cost option if compared to other designs. Depending on the construction, the external gear motors are able to operate bidirectionally, in other words, it can work as a pump or motor (from now on, they will be referred as pump/motors).

The pump/motors were selected according to the area ratio of the cylinder. The decision was made based on the pump/motor sizes available in the market and on the relation given by

$$\frac{D_B}{D_A} \cong \frac{A_B}{A_A}, \quad (3.1)$$

where D_A and D_B are the volumetric displacements of the pump/motors in A- and B-sides, respectively, and A_A and A_B the corresponding cylinder chamber area.

The pump/motors utilized in the setup were the Bosch Rexroth AZMF-12-008UCB20PX and AZMF-12-011UCB20PX. Table 3.3 presents the main parameters of the components.

Table 3.3 - Main parameters of the external gear motors.

Model	AZMF-12-008UCB20PX	AZMF-12-011UCB20PX
Displacement	8 cm ³ /rev	11 cm ³ /rev
Maximum continuous pressure	250 bar	250 bar
Minimum speed	700 rpm	600 rpm
Maximum speed	4000 rpm	3500 rpm

Source: Bosch Rexroth external gear motor data sheet.

3.1.3 Hydraulic accumulator

The hydraulic accumulator utilized is a diaphragm type for its practicality, compact design, and fast dynamic response. As the system is closed the accumulator has the duty to provide or store fluid, that is, a pressurized reservoir. For the setup, a 0.7 liter accumulator was installed (code: HAD0.7-250-1X/80G04A-1N111-BA), and the gas pressure was set in 2 bar.

3.1.4 Hydraulic cylinder

The actuator is an asymmetrical cylinder, MIRO C-10-60/30x400, and its parameters are shown in Table 3.4. Mechanical losses, caused by friction, are presented in Section 4.5.1 and internal leakage through the piston sealing was ignored in this study.

Table 3.4 - Main parameters of the linear actuator.

Parameter	Value
Maximum Pressure	190 bar
Piston head diameter	60 mm
Piston rod diameter	30 mm
Stroke	400 mm
Inlet diameter (Piston head side)	11 mm
Inlet diameter (Piston rod side)	12 mm

Source: Adapted from Järf (2016).

3.1.5 Valves

The system is equipped with four valves, two relief valves for safety purpose, and two check valves to avoid cavitation. The check valves were considered necessary especially when the cylinder in

retracting due to the pump/motor of the rod side line is providing less fluid than required by the cylinder chamber, dropping the pressure. The relief valves are Bosch Rexroth relief valve 04.11.18039910000 with an adjustment pressure range from 30 to 100 bar. The check valves are Argus nonreturn valves with an opening pressure of 0.5 bar.

3.2 SENSORS

In this section the pressure and position sensors utilized to capture data from the experiment are presented.

3.2.1 Pressure transmitters

Three pressure transmitters were installed in the test bench to obtain the pressure values during the motion of the actuator. Two of them are situated in the chamber lines of the cylinder and the third is monitoring the accumulator line. The sensors in the chamber lines are the Trafag NAT250.0A with a pressure range of 0 to 250 bar. In the accumulator line, a Trafag NAT16.0A is utilized with a range of 0 to 16 bar. These transmitters have an output signal from 4 to 20 mA, the accuracy of ± 0.5 bar, and maximum overpressure three times the highest pressure able to read.

3.2.2 Wire incremental encoder

The position of the cylinder is measured through a wire actuated encoder. The encoder is attached to the cylinder and the wire at the same fastening point of the cylinder on the crane. This manner is possible to monitor the piston position. The sensor utilized is a SIKO SGI wire incremental encoder (code: SGI-3500-0-SK-S-JA). This information was found in Järf (2016). However, the encoder type is no longer produced and no more information is available.

3.3 ELECTRIC COMPONENTS

The electric components are the frequency converter which runs the electric motor, and the data acquisition system which records and reads the sensor data.

3.3.1 Frequency converter

The electric motor driver is a Bosch Rexroth Indradrive C-HCS02.1E-W0028 frequency converter. The motor control signals are sent to the driver and the computer receives information back such as rotational frequency and estimated torque.

3.3.2 Data acquisition card and control system

Two data acquisition cards are utilized, a National Instrument NI USB-6009 and NI USB-6218. The USB-6009 provides 8 single-ended analog input channels, 12 digital inputs/outputs channels, 2 analog outputs channels. Analog input resolution of 14 bits differential and 13 bits single-ended. The NI USB-6218 card has 16 differential or 32 single-ended analog input channels, with a resolution of 16 bits, 2 analog outputs (16 bits), and 8 digital input/output channels. The devices are connected via USB to the computer with the LabVIEW software. A program in LabVIEW platform is responsible to process and data logging as well as to send the control signal to the electric motor.

4. MODELING DESCRIPTION

In this section, the simulation model made in order to investigate the behavior of the system is described. As the intention is analyzing the weakest part of the system in an energy efficiency point of view, just the hydraulic system has been modeled. The input signal is given by rotational frequency provided by the electric motor, and outputs are cylinder position, the required torque, and the pressure in the chambers.

Hoses and cylinder chambers are fluid volumes represented by the continuity equation, written as

$$\frac{dp}{dt} = \frac{\beta_{eff}}{V_0 \pm Ax} \left(\Delta q_V - A \frac{dx}{dt} \right), \quad (4.1)$$

where dp/dt is the pressure derivative inside the closed volume, β_{eff} is the fluid effective bulk modulus [Pa], V_0 is the initial volume [m^3], Δq_V is the difference between inlet and outlet flow rates, A for cylinder transversal area, x is the cylinder position and dx/dt the velocity. For hoses, the Equation (4.1) is simplified by $dx/dt = 0$.

The flow restriction is also needed to be considered, such as throttle valves and orifices. The flow rate through the orifice (q_{Vo}) is given by

$$q_{Vo} = CdA_o \sqrt{\frac{2\Delta p}{\rho}}, \quad (4.2)$$

where Cd the discharge coefficient, A_o the area of the orifice, ρ the fluid density [kg/m^3] and Δp the pressure difference over the orifice. For simplification purposes, the flow through the orifice will be also calculated linearly such as:

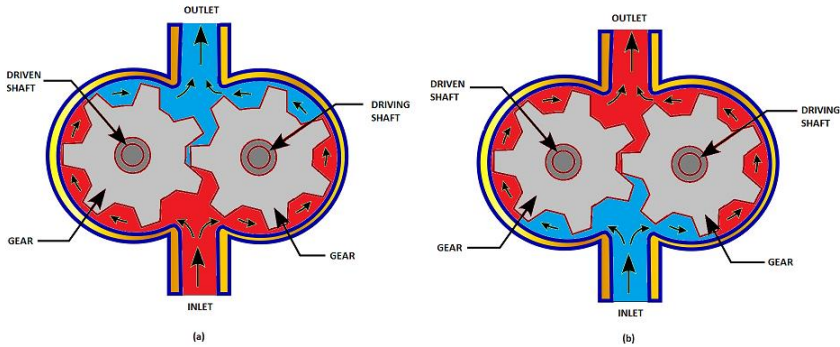
$$q_{Vo} = K_V \Delta p, \quad (4.3)$$

where K_V is volumetric coefficient for the orifice.

4.1 PUMP/MOTOR MODEL

Bidirectional external gear motors were selected for this application due to its possibility of working also as a pump when the shaft direction is reversed, its robustness, and especially for the lower costs comparing with other pump/motor principles. These components are commonly applied for fluid power transmissions, automotive, and aerospace due to their advantages of low manufacturing cost, compact units, energy efficiency and good tolerance to contamination (ZHAO & VACCA, 2017). An external gear pump/motor schematic is shown in Figure 4.1.

Figure 4.1 - External gear pump/motor schematic. (a) Motor mode and (b) pump mode.



Source: Adapted from www.daerospace.com.

4.1.1 Pump/motor flow rate

The theoretical volumetric flow rate produced by the pump/motor is found by

$$q_{vt\ pm} = D_{pm} \omega_{pm} \quad (4.4)$$

where ω_{pm} is the angular speed of the pump/motor [rad/s], and D_{pm} the volumetric displacement [m^3/rad].

The hydraulic power delivered to the fluid is less than the in mechanical power due to losses caused by internal leakage, external leakage, pump cavitation, partial filling of the pump, fluid compressibility, and friction. The leakages are a function of the

differential pressure over the pump/motor and the viscosity of the fluid, which is directly affected by the oil temperature (MANRING, 2005). For this reason, the pump/motor volumetric flow rate is estimated as

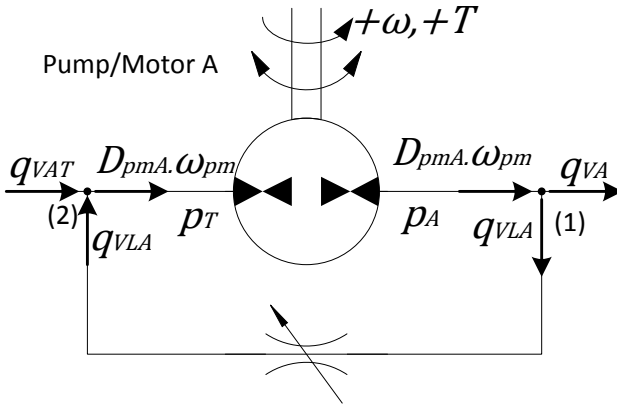
$$q_{Vpm} = D_{pm}\omega_{pm} - q_L(\Delta p, \omega), \quad (4.5)$$

being the sum of leakages, q_L a function of differential pressure and angular speed.

The leakage coefficients were determined according to the catalog information. This approximation is far from being exact, taking into account that the volumetric efficiency of the pump/ motor varies in function of the pressure difference, angular speed, and temperature of the fluid. The exact coefficients for the leakage can be calculated by measurements in different conditions with an appropriate test bench, which was not the case. So, constant coefficients were utilized based on the catalog information of the components for a specific rotational speed and pressure. The approximated values of volumetric efficiency provided by the manufacturer were used and the simulation represented relatively well the experimental data of the whole system.

The leakage in the pump/motors is represented by a constraint in parallel. The equations utilized to model the leakage are presented next and are based on the Equation (4.3). Figure 4.2 shows the pump/motor (component number (2) in the Figure 3.1) acting on the piston side, and Figure 4.3 shows the pump/motor (component number (3)) at the piston rod side. The following equations represent the inlet and outlet flow rates in each control volume. The continuity equation for a very small control volume is utilized to demonstrate the flow directions and to equate correctly the signs of the leakage in each pump/motor. The positive flow rate is indicated by the arrows. When the flow rate results in a negative value, the flow rate is going to the opposite direction.

Figure 4.2 - Diagram of the pump/motor at the piston side.



Source: Author.

At point (1)

$$-q_{VA} - q_{VLA} + D_{pmA} \cdot \omega_{pm} = 0$$

$$q_{VA} = D_{pmA} \cdot \omega_{pm} - K_{LA} \cdot (p_A - p_T), \quad (4.6)$$

where q_A is the flow rate going to the cylinder chamber (piston side), q_{VLA} is the volumetric flow rate corresponding to the leakage that is represented by a coefficient K_{LA} and the pressure difference between the pressure in the cylinder chamber, p_A , and the pressure in the reservoir (or accumulator line), p_T .

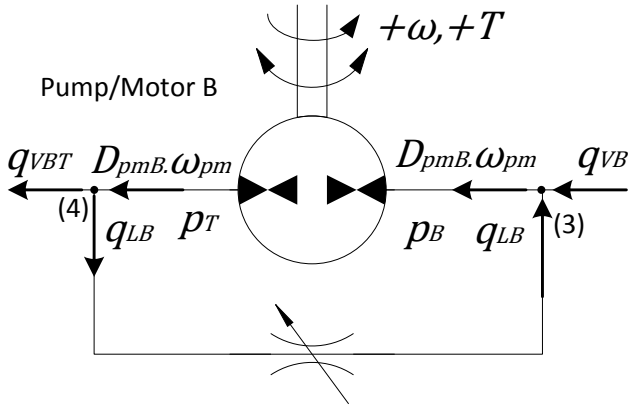
At point (2)

$$+q_{VAT} + q_{VLA} - D_{pmA} \cdot \omega_{pm} = 0$$

$$q_{VAT} = D_{pmA} \cdot \omega_{pm} - K_{LA} \cdot (p_A - p_T) \quad (4.7)$$

where q_{VAT} is the flow rate leaving the control volume of the accumulator line through the pump/motor A.

Figure 4.3 - Diagram of the pump/motor at the piston rod side.



Source: Author.

At point (3)

$$q_{VB} + q_{VLB} - D_{pmB} \cdot \omega_{pm} = 0$$

$$q_{VB} = D_{pmB} \cdot \omega_{pm} - K_{LB} \cdot (p_T - p_B), \quad (4.8)$$

where q_{VB} is the flow rate going out of the cylinder chamber (rod side chamber), q_{VLB} is the volumetric flow rate corresponding to the leakage at the pump/motor B, represented by the coefficient K_{LB} and the pressure difference between the reservoir line and the rod side chamber, p_B .

At point (4)

$$-q_{VBT} - q_{VLB} + D_{pmB} \cdot \omega_{pm} = 0$$

$$q_{VBT} = D_{pmB} \cdot \omega_{pm} - K_{LB} \cdot (p_T - p_B). \quad (4.9)$$

where q_{VBT} is the flow rate entering in the control volume of the accumulator line through the pump/motor B. The K_{LA} [$\text{m}^3/\text{Pa}\cdot\text{s}$] and K_{LB} [$\text{m}^3/\text{Pa}\cdot\text{s}$] are represented by linear equations as a function of the angular speed, ω . The coefficients are given by

$$K_{LA} = 1.60404x10^{-12} - 2.559x10^{-14} \cdot |\omega| \quad (4.10)$$

and

$$K_{LB} = 14x10^{-12} - 2.515x10^{-13} \cdot |\omega|. \quad (4.11)$$

These equations were an approximation based on the volumetric efficiency given by the catalogue at a certain angular speed and considering that the efficiency decreases with the decreasing of the angular speed. This explains the minus signal in the Equations 4.10 and 4.11. This way it was possible to represent the effect of the small rotational speed in the pressure measurements. This assumption was based on experimental observations carried out in LASHIP found in Dalla Lana (2005) and Dalla Lana & De Negri (2006).

4.1.2 Pump/motor torque

The torques required (T_{req}) and provided (T_{pro}) by the pump/motors are calculated by the equations:

$$T_{req} = \frac{\Delta p D_{pm}}{\eta_{hm}}, \quad (4.12)$$

and

$$T_{pro} = \Delta p D_{pm} \eta_{hm}, \quad (4.13)$$

where η_{hm} is the mechanical efficiency of the pump/motor. This value will be used as a constant, due to torque losses caused by friction are not been detailed in this work.

4.2 EFFECTIVE BULK MODULUS

The fluid compressibility is an important parameter inside the system. Defined as the ability of it to change its volume when its pressure varies, it has a direct impact on the transient behavior of hydraulic systems (RABIE, 2009).

The effective bulk modulus represents the total compressibility of the system. According to Gholizadeh *et al.* (2014), temperature, pressure and the air content in the oil affect its value, also there are three different

ways for the air present itself inside the system, as “lumped air”, a large bubble at the top of oil column, as small bubbles distributed all over the system or dissolved air.

To include the effect of compressibility in the system, the bulk modulus of the liquid, gas, and the hoses and pipelines are combined in the equation for the effective bulk modulus given by:

$$\beta_{eff} = \frac{1}{\frac{1}{\beta_H} + \frac{1}{\beta_l} + \left(\frac{V_g}{V_t}\right) \frac{1}{\beta_g}} \quad (4.14)$$

where β_H is the bulk modulus of the hoses and connections, β_l the bulk modulus of the hydraulic fluid, V_g is the of air trapped in the system, V_t represents the total volume, and β_g is the bulk modulus of the gas. Considering an adiabatic process, in which the heat is transferred through the wall of the system, the bulk modulus of the gas is considered the same value as the pressure at the moment analyzed (LINSINGEN, 2016).

Most of the hydraulic circuits utilize rubber hoses with steel wire braid. The hoses provide flexibility when mounting the circuit; however, they reduce significantly the bulk modulus of the system. According to McCloy and Martin (1980, *apud* Linsingen, 2016), the values for rubber hoses can be considered between 70 MPa and 350 MPa. Another reference, such as Stringer (1976), the limit for bulk modulus in flexible hoses can reach 700 MPa depending on the manufacturer.

The bulk modulus of the fluid for the simulation was estimated at 1400 MPa, the value varies according to the fluid composition and temperature. The hydraulic oil used in the system is mineral oil type (super 32). Table 4.1 presents types of fluid utilized in hydraulic systems depending on the industry sector.

Table 4.1 - Typical values for hydraulic fluids properties.

Properties (Typical values)	Mineral oil	HFA	HFB	HFC	HFD
Density (15°C) [kg/m ³]	850/930	≈1000	≈950	≈1050	1050/1400
Bulk Modulus (40°C) [N/m ²]	1,48/2,1 x10 ⁹	2x10 ⁹	2,2 x10 ⁹	2 x10 ⁹	2,2/2,6 x10 ⁹

Source: Adapted from Linsingen (2016).

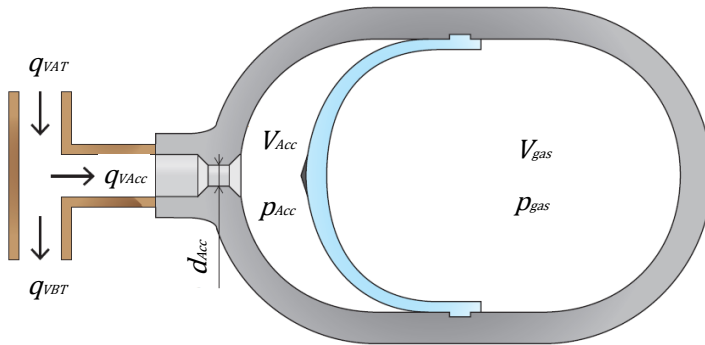
- HFA (or HWCF-High) - water content fluid (90% or more).
- HFB - Water in oil (40-60%).
- HFC - Water glycols (35-45%).
- HFD - Synthetic fluid (no water).

4.3 HYDRAULIC ACCUMULATOR MODEL

Hydraulic accumulators are used to storing or providing fluid in certain pressure in order to minimize sudden pressure spikes, caused by an external force, or supply a short-duration flow demand (TOTTEN and DE NEGRI, 2011, Ch. 1).

In Figure 4.4 the inlet and outlet flow rates of the diaphragm-type hydraulic accumulator.

Figure 4.4 - Accumulator flows schematic.



Source: Adapted from Järf (2016).

From the continuity equation for a small control volume

$$q_{VAcc} = q_{VAT} - q_{VBT} \quad (4.15)$$

where q_{VAcc} is the volumetric flow of accumulator, q_{VAT} the volumetric flow rate coming from pump/motor A and q_{VBT} the volumetric flow rate going to the pump/motor B.

Using the ideal gases relation (RABIE, 2009), it is possible to represent the accumulator gas volume and pressure as a function of pre-charge pressure (p_{Acc}) and volume (V_{Acc}) of the accumulator as given:

$$p_{gas}V_{gas}^\gamma = p_{Acc}V_{Acc}^\gamma \quad (4.16)$$

which γ is the adiabatic constant. Therefore, the fluid pressure in the accumulator is:

$$p_{fluid} = p_{Acc} = \frac{p_{gas}V_{gas}^\gamma}{V_{Acc}^\gamma} + p_{HS}. \quad (4.17)$$

The p_{HS} is called by Järf (2016) as the hard-stop contact pressure, when the accumulator is almost empty and the diaphragm reach the wall, in other words, the end stop. The hard-stop pressure is calculated by the following rules

$$p_{HS} = \begin{cases} -K_s V_{gas}, & \text{if } V_{gas} > 0.99V_{Acc}, \\ 0, & \text{otherwise.} \end{cases} \quad (4.18)$$

where K_s is a proportional constant.

The reason for the negative signal could be physically explained when the diaphragm reaches the orifice of the accumulator, it means there is no pressure from the fluid resisting to the diaphragm expansion. However, this phenomenon was not detected during the simulation and also because the accumulator volume is bigger than the minimum size required, such that there is always fluid inside it. The minimum volume should be at least the volume of the piston rod (the volume difference between the chambers). More information about the accumulator model can be found in Järf (2016). The volume of gas can be found by

$$V_{Acc} = V_{gas} + V_{fluid}, \quad (4.19)$$

and considering that the volume in the accumulator is the integration with respect to time to the volumetric flow rate in the accumulator

$$V_{fluid} = \int q_{V_{Acc}}. \quad (4.20)$$

4.4 ORIFICE MODEL

The inlet of the accumulator is modeled separating the control volumes of the accumulator and the hoses that connect it to the pump/motors. According to Ellman & Piché (1996), when the orifice

flow rate is modeled using the conventional equation for all pressures (see Equation 4.2), the solver fails due to its adaptive time step mechanism. In order to avoid error during simulation when pressure drops to near zero, a modified formula is proposed by Ellman & Piché (1996) is given by:

$$q(\Delta p) = \begin{cases} C_{turb} A_o \sqrt{\frac{2\Delta p}{\rho}}, & (p > p_{tr}) \\ \frac{3A_o v R_{tr}}{4d_o} \left(\frac{\Delta p}{p_{tr}}\right) \left(3 - \frac{\Delta p}{p_{tr}}\right), & (0 \leq p \leq p_{tr}) \end{cases} \quad (4.21)$$

where C_{turb} is the turbulent discharge coefficient, A_o the orifice area, Δp the pressure difference over orifice, ρ and v are density and kinematic viscosity of the fluid, respectively, R_{tr} is the transition Reynolds number, d_o orifice diameter and p_{tr} is the transition pressure, which is given by

$$p_{tr} = \frac{9R_{tr}^2 \rho v^2}{8C_{turb}^2 d_o^2}. \quad (4.22)$$

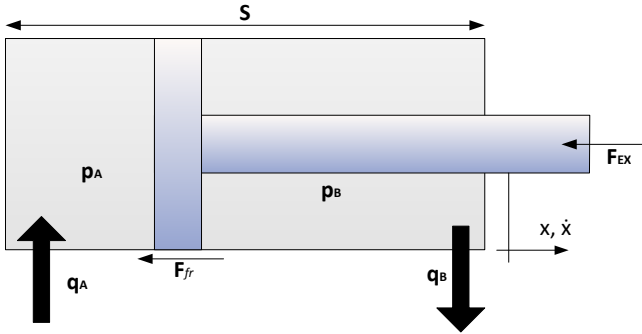
The values for negative pressure differences are specified by the condition

$$q(-\Delta p) = -q(\Delta p). \quad (4.23)$$

4.5 CYLINDER MODEL

Hydraulic cylinders are linear actuators, which turns hydraulic power into mechanical power. An asymmetrical cylinder is used in this work once its current application is the mobile machine industry and these type of cylinders are more compact comparing to symmetric ones. It is represented by two different volumes (A- and B-Chamber) which vary depending on the piston position as shown in Figure 4.5.

Figure 4.5 - Hydraulic cylinder schematic.



Source: Author.

The volume A shown in Figure 4.5 is a function of the piston head area A_A , the position of the piston x , and its dead volume (gap between the piston and wall, and inlet orifice), V_{0A} . The volume B is the same, but it needs to consider the rod volume inside the chamber. Therefore, when the piston is moving, the flow rate q_A and q_B are not the same. Volumes are given by

$$V_A = V_{0A} + A_A x, \quad (4.24)$$

and

$$V_B = V_{0B} + A_B (S - x), \quad (4.25)$$

where S is the stroke length.

The pressure variation in chambers A and B are calculated by the continuity equation for the control volume and using Equation (4.24) and Equation (4.25), finally results in

$$\frac{dp_A}{dt} = \frac{\beta_{eff}}{V_{0A} + A_A x} \left[q_A - K_L (p_A - p_B) - A_A \frac{dx}{dt} \right], \quad (4.26)$$

$$\frac{dp_B}{dt} = \frac{\beta_{eff}}{V_{0B} + A_B (S - x)} \left[-q_B + K_L (p_A - p_B) + A_B \frac{dx}{dt} \right]. \quad (4.27)$$

In this model, the internal leakages are not considered, so the leakage coefficient K_L is 0.

The cylinder force (or external force), F_{Cyl} is composed of hydraulic force provided by the cylinder is given by the force differences between A and B chamber, also there is a restrictive force caused by friction F_{fr} , between the cylinder wall and the piston head, as seen in

$$F_{Cyl} = p_A A_A - p_B A_B - F_{fr} - F_{end}, \quad (4.28)$$

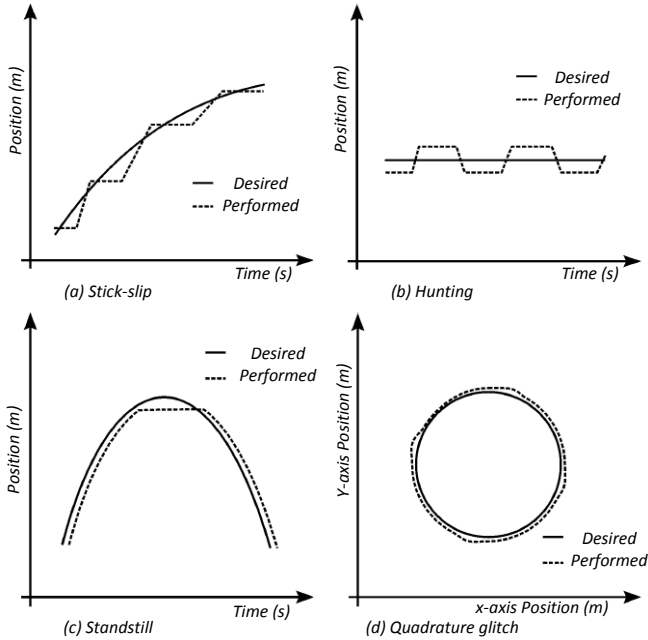
where F_{end} is the end force or the wall force when the actuator reaches the limits of its stroke. The inertia will be presented in the Section 4.6 where the load model is detailed.

4.5.1 Friction force

The friction force is one of the most important nonlinearities found in controlling mechanical systems. It decreases the force or torque available at the actuator, and losses can reach up to 30 % (DUPONT, 1993, *apud* BONCHIS et al, 1999). According to Armstrong & Canudas-de-Wit (1996, *apud* VALDIERO, 2005), different effects can compromise the performance of the motion. These effects are called stick-slip, hunting, standstill and quadrature glitch (see Figure 4.6). The stick-slip (a) refers to a variation of slip movement and standstill. The hunting (b) occurs when the motion oscillates between a constant reference position. The standstill (c) is the friction effect when the system decelerates for a certain time when passing through null speed. Finally, the quadrature glitch (d) is the error when the two-axis machine fails to precisely track the desired motion. For this reason, it is necessary a mathematical model to calculate the magnitude of friction force acting on the actuator.

The friction of a hydraulic cylinder is dominated by the friction between the piston/rod seals and contacting surfaces. Each material of seals has its specific viscoelastic characteristics and consequently affects the friction of the hydraulic cylinder. In addition, the pressures acting on the seals cause deformation of the seals and affect the friction characteristics (TRAN *et al.*, 2012).

Figure 4.6 - Effects on the motion performance caused by friction forces.



Source: Armstrong & Canudas-de-Wit (1996, *apud* VALDIERO, 2005).

Utilized in many hydraulic and pneumatic applications, such as Teixeira (2015), Vígolo (2018), and so on, the LuGre model is implemented in this study to estimate the friction behavior. The LuGre model is presented in Canudas-de-Wit *et al* (1995), where the mechanisms of friction are represented by the contact of two rigid bodies through elastic bristles (see Figure 4.7). When a tangential force is applied, the bristles deflect like springs increasing the friction force. Once the force is sufficiently large, the bristles deflect in a way that the can slip.

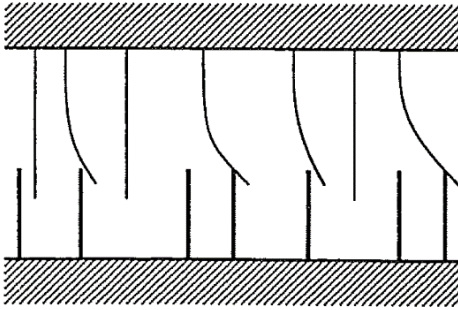
The average deflection of the bristles is characterized by z and the deflection rate (dz/dt) is given by

$$\frac{dz}{dt} = v - \frac{\sigma_0 z}{g(v)} |v|, \quad (4.29)$$

where v is the relative velocity between the two surfaces, σ_0 is the stiffness of the elastic bristles, and $g(v)$ is a positive function and

depends, for instance, on material properties, lubrication, and temperature.

Figure 4.7 - Contact between bristles of two surfaces.



Source: Canudas-de-Wit *et al* (1995).

The friction force is defined by

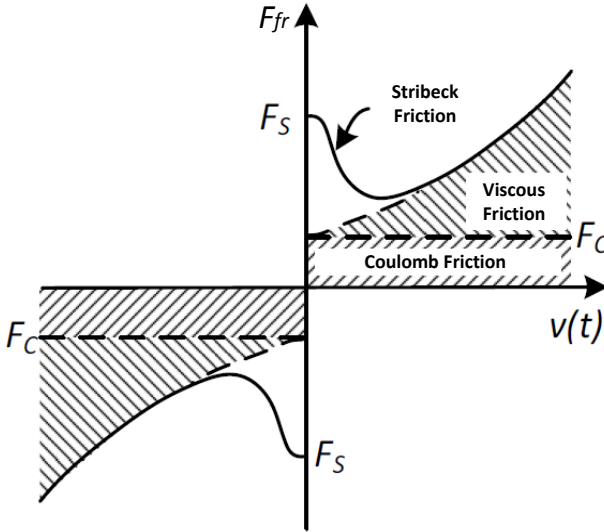
$$F_{Fr} = \sigma_0 z + \sigma_1 \frac{dz}{dt} + \sigma_2 v, \quad (4.30)$$

where σ_1 is the damping coefficient and σ_2 is a viscous friction coefficient proportional to the relative velocity. Combining the equations (4.29) and (4.30), the steady-state friction force is measured in when v is constant, resulting in

$$F_{steady-state} = g(v) \operatorname{sgn}(v) + \sigma_2 v. \quad (4.31)$$

The function $g(v)$ is determined according to the static friction map. The behavior of static friction in relation to the relative velocity combines the static friction force, the Stribeck region, the Coulomb friction force, and viscous friction (Teixeira, 2015). Figure 4.8 presents the friction curve in steady-state.

Figure 4.8 - Friction map in terms of Stribeck, Coulomb and viscous friction.



Source: Adapted from Valdiero (2005).

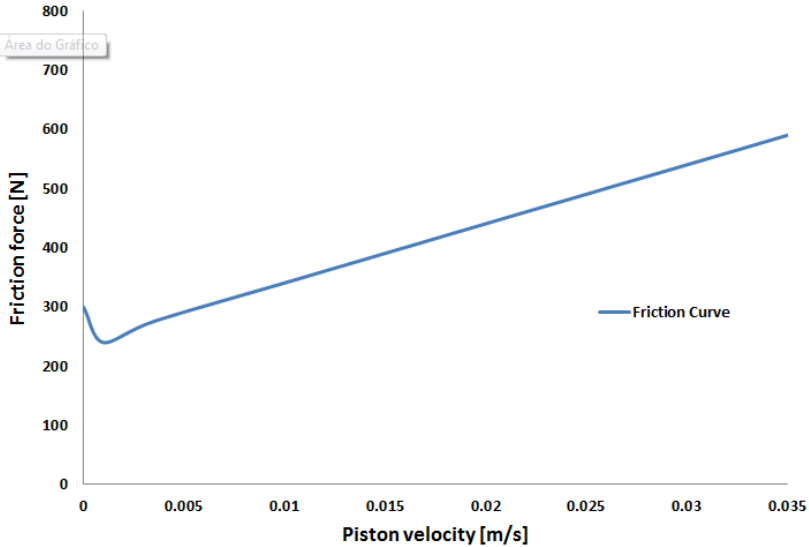
Thus the equation for $g(v)$ is given by:

$$g(v) = F_c + (F_s - F_c)e^{-\left(\frac{v}{v_s}\right)^2}, \quad (4.32)$$

where F_c is the Coulomb friction force, F_s is the static friction force and v_s is the Stribeck velocity.

The parameters considered in this model were initially based on the experiments performed by Järf (2016) who utilized the same actuator in his research; however, the friction coefficients did not fit well for the experiments made in this work. In order to match and better represent the pressure curves of the model with the experiment some parameters were adjusted, in particular Coulomb and viscous friction. The decision of not using the coefficients identified by Järf was made due to the lack of information in his report about the conditions the test was submitted. Also the information available was only for positive velocities. In this case, the friction is considered symmetric for both positive and negative velocities of the cylinder. Figure 4.9 shows the friction curve utilized for this work.

Figure 4.9 - Friction curve adopted in the simulation.



Source: Author.

Table 4.2 summarizes the friction parameters estimated according to the measurements presented in Figure 4.9.

Table 4.2 - Friction parameters.

Parameter		Coefficient values	Unit
Stiffness coefficient	σ_0	300000	N/m
Damping coefficient	σ_1	547.72	Ns/m
Viscous friction coefficient	σ_2	10000	Ns/m
Coulomb friction	F_c	240.61	N
Static friction	F_s	300	N
Stribeck velocity	v_s	0.0005	m/s

Source: Author.

4.5.2 End force

As mentioned before, this force is added in the Equation (4.28) in order to limit the cylinder position in a range position from $0 \leq x \leq S$. This force needs to be modeled with caution to avoid any undesirable effect or numeric error during simulation. It is determined based on the

elastoplastic theory of materials model (BACCA *et al.* 2010). This theory is assumed that the force has a mass-spring-damper system behavior, and the force is represented as

$$F_{end} = \begin{cases} k_{end}x + \zeta_{end}\dot{x}, & \text{if } x < 0 \\ k_{end}(x - S) + \zeta_{end}\dot{x}, & \text{if } x > S \end{cases} \quad (4.33)$$

where k_{end} is the stiffness constant and ζ_{end} the damping constant.

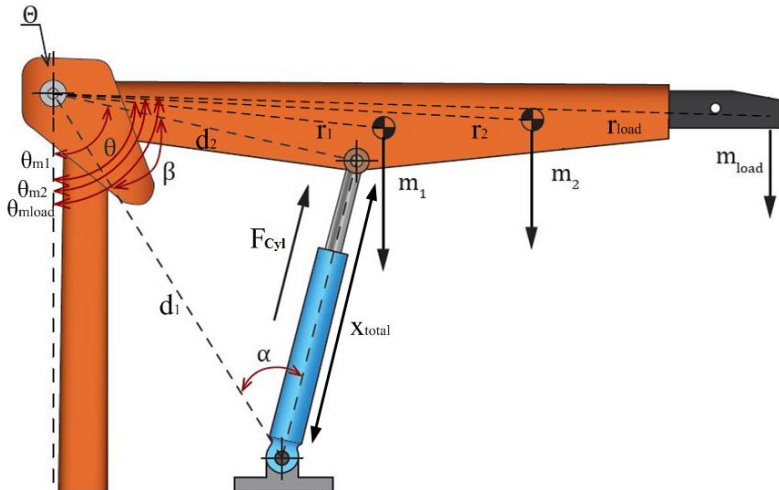
4.6 LOAD

To represent the load force applied in the system, it is necessary to utilize the free body diagram of the crane structure. The force acting on the boom generates a torque around the joint Θ , determined by the Newton's second law:

$$\sum M_{\Theta} = J \frac{d^2\theta}{dt^2} \quad (4.34)$$

where M_{Θ} is the torque on the joint, J is the moment of inertia of the boom and load and $d^2\theta/dt^2$ is the angular acceleration. Figure 4.10 shows the crane and the actuator attached.

Figure 4.10 - Free body diagram of the crane.



Source: Adapted from Järf (2016).

From Figure 4.10 the torque is given by

$$\frac{d^2\theta}{dt^2} = \frac{(-m_1 \cdot r_1 \cdot \text{sen}(\theta_{m1}) - m_2 \cdot r_2 \cdot \text{sen}(\theta_{m2}) - m_{load} \cdot r_{load} \cdot \text{sen}(\theta_{mload}))g + F_{Cyl} \cdot \text{sen}(\alpha) \cdot d_1}{J}, \quad (4.35)$$

where m_1 and m_2 are the mass of the segment the crane is composed of, r_1 and r_2 are the distance between the centre of mass of each segment and the joint, θ_{m1} and θ_{m2} are the angle between the center of mass and the reference perpendicular axis, and g is the gravitational constant. For simplification, the load is considered at the point the chain is attached to the movable part, so m_{load} considers the mass of the load, chain and the hook. F_{Cyl} is the hydraulic force, α is the angle between the cylinder and the joint, and d_1 the distance.

As the angle β is around the same axis as angle θ , solving the differential equation 4.35 it is possible to calculate the angles α and β using the follow equation:

$$\beta = \beta_0 + \int_0^t \frac{d\theta}{dt} dt, \quad (4.36)$$

where β_0 is the initial angle when the cylinder is fully retracted and t the simulation time. The angle α then is determined with the sine rule given by

$$\text{sin}(\alpha) = \frac{d_2}{x_{total}} \text{sin}(\beta), \quad (4.37)$$

where d_2 is the distance of the upper fastening point of the cylinder and the joint. x_{total} is the length of the cylinder plus the displacement of the stroke. To obtain the x_{total} is utilized the cosine rule as follow

$$x_{total}^2 = d_1^2 + d_2^2 - 2d_1d_2\text{cos}(\beta), \quad (4.38)$$

so x_{total} is defined as

$$x_{total} = \sqrt{d_1^2 + d_2^2 - 2d_1d_2\text{cos}(\beta)}. \quad (4.39)$$

Deriving the equation 4.39 in function of time t , being β also a function of time as shown in equation 4.36, is obtained the velocity of the cylinder.

$$\frac{dx}{dt} = \frac{d_1 d_2 \frac{d\beta}{dt} \sin(\beta)}{\sqrt{d_1^2 + d_2^2 - 2d_1 d_2 \cos(\beta)}}. \quad (4.40)$$

The masses m_1 and m_2 were obtained through selecting the material in the 3D model built by Järf (2016) in PTC Creo Parametric 3.0 software. The positions of the centre of masses were also estimated according to the geometry of the crane model. The moment of inertia is determined by

$$J = \sum m_i r_i^2. \quad (4.41)$$

4.7 CHECK VALVE MODEL

The check valve was modeled as an orifice utilizing the Equation (4.3). The valve only allows flow in one direction, from the accumulator line to the chambers. The volumetric flow rate through the check valve is given by

$$q_{CV} = \begin{cases} K_V(\Delta p - p_{cp}), & \Delta p - p_{cp} \geq 0 \\ 0, & \Delta p - p_{cp} < 0 \end{cases} \quad (4.42)$$

where K_V is the volumetric coefficient of the orifice in the check valve, Δp is the difference between the reservoir line pressure and the chambers, $(p_T - p_A)$ or $(p_T - p_B)$, and p_{cp} is the cracking pressure of the valve spring.

To estimate the K_V value, a curve of a check valve with similar size from other manufacturer was utilized (see Appendix B). From the curve (Flow Rate x Pressure Difference), an approximated linear equation is plotted over the curve and the angular coefficient (α_{CV}) value is found. The K_V is calculated by

$$K_V = \frac{1}{\alpha_{CV}} = 5.632e^{-10}. \quad (4.43)$$

5. VALIDATION OF THE MODEL

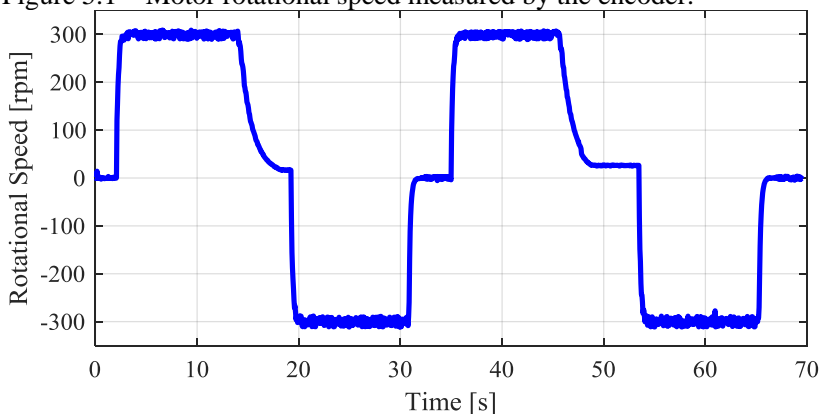
This chapter presents the validation of the model using the data obtained from the experiments with the test bench and how they were utilized to set correct parameters of the components.

Firstly, 40 kg of weight (392 N) was added at the end of the crane arm, this load was chosen in a conservative manner and utilized also to model the load acting on the actuator.

The input signal given by the controller is the electric motor rotational frequency. In this case, it is an open-loop control system and the signal to run and stop is sent manually. Figure 5.1 shows the electric motor rotational speed measurements where two cycles of lifting and lowering the crane without reaching the final position of the actuator were performed. The motor rotational speed data will be utilized as an input signal in the model in order to not be necessary to include the model of the electric motor.

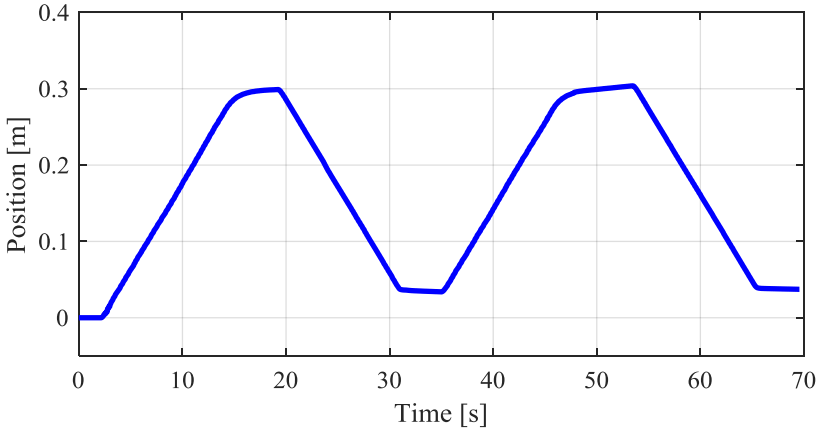
Figure 5.2 presents the measured position of the actuator. The cylinder position data was utilized as assistance to set the real volumetric displacement and approximate leakage coefficient for the piston side pump/motor. Even obtaining the theoretical volumetric displacement value from the catalog (see Table 3.3), the real value can vary. In the simulation, the volumetric displacement of the piston side pump/motor and the rod side pump/motor are 13.03 cm³/rev and 9.35 cm³/rev, respectively.

Figure 5.1 – Motor rotational speed measured by the encoder.



Source: Author.

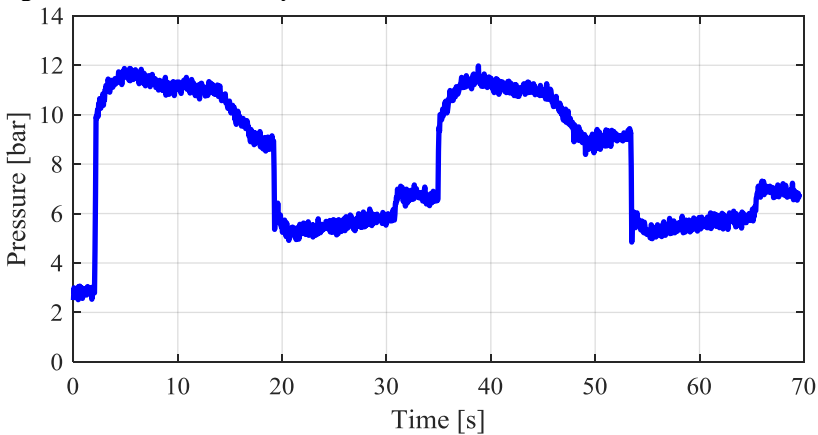
Figure 5.2 - Cylinder position in the performed cycles.



Source: Author.

As it can be seen from Figure 5.2, it was avoided to reach its full stroke length in order to not produce any pressure spikes due to the end force and analyze the pressure behavior without this phenomenon. In this work, the pressure data was used to validate the model. Figure 5.3 shows the pressure variation in the piston side volume along the cycle. This side of the circuit will handle the highest pressures in the system once that the load force is always acting in the same direction, compressing the control volume.

Figure 5.3 - Pressure in the piston side volume.

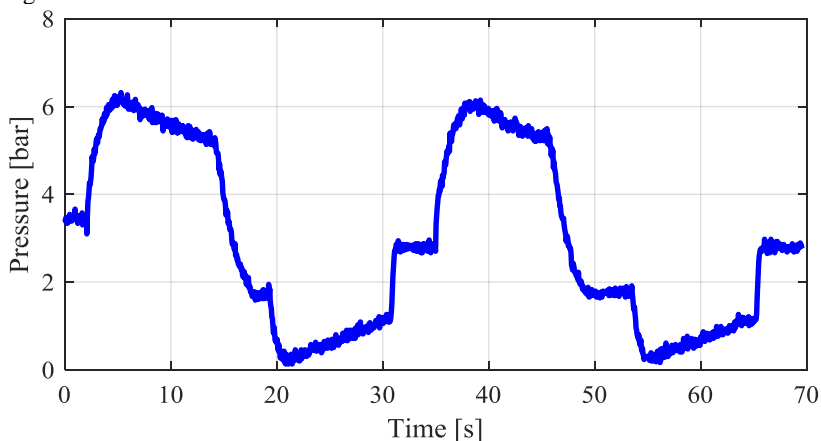


Source: Author.

In Figure 5.4 the pressure in the rod side chamber is presented. It is noticed that when the crane is lifting, even that the pump/motor works to pump fluid out of the chamber, it builds an increase in the pressure, meaning that the pump/motor volumetric displacement should be a little higher. During the lowering motion it is also visible that the pump/motor is smaller than it should be for this specific cylinder, causing the accented drop of pressure in the chamber at the time the electric motor is reversed (19 sec. and 53 sec.). This will be discussed forward in the end of this chapter.

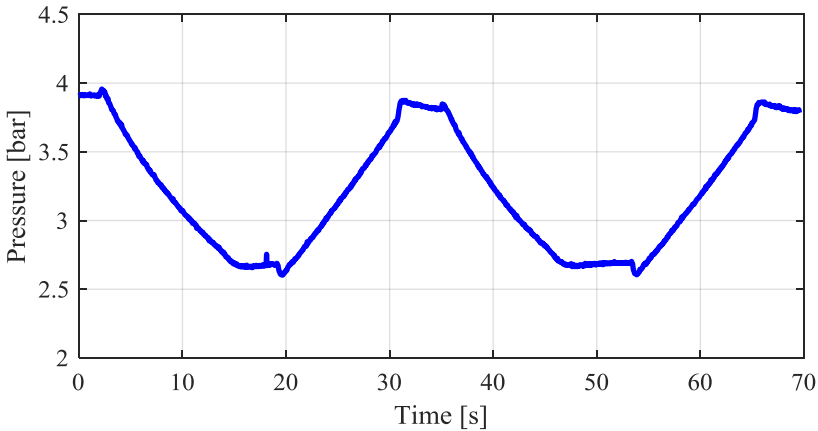
At last, Figure 5.5 shows the pressure variation at the accumulator line along the cycle. The accumulator empties when lifting the load and is filled when lowering, which was expected. The model validation was fundamentally based on the pressure data, no volumetric flow rate and torque sensors were available at the time of the tests.

Figure 5.4 - Pressure level in the rod side volume.



Source: Author.

Figure 5.5 - Pressure level in the accumulator line.

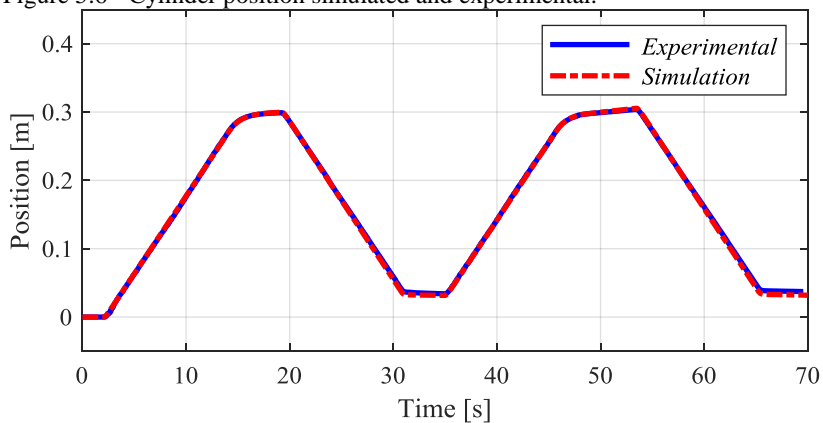


Source: Author.

As the system is a closed-circuit, a small change of pressure in one side of the system affects the others significantly. The parameters that have the most impact during the parameterization of the model were definitely the pump/motors displacements and their respective leakage coefficients. The leakage coefficients were estimated (see Equation 4.10 and 4.11) starting from the catalogue information and adjusted to better fit the experimental data curves. The results obtained by the mathematical model presented a certain convergence and similar behavior as the experiment.

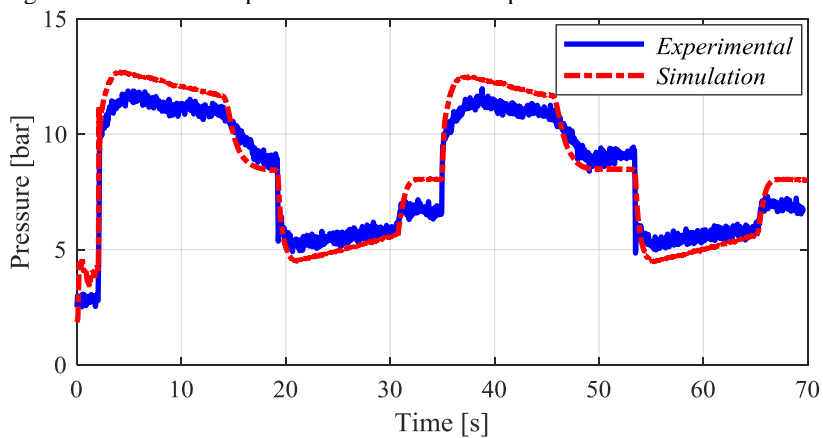
Figure 5.6 shows the cylinder position in the model follows correctly the reference position. With the motion well performed it is possible to look at the pressure of the chamber in the model and compare to the test bench. Figure 5.7 presents the piston side pressure for both simulation and experiment.

Figure 5.6 - Cylinder position simulated and experimental.



Source: Author.

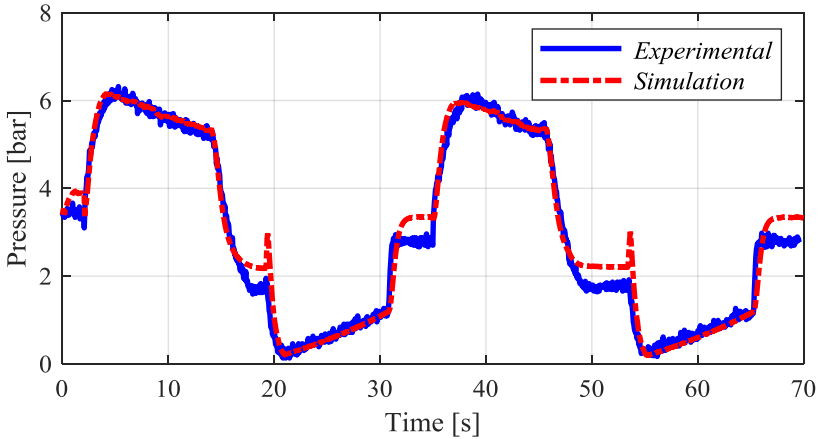
Figure 5.7 - Piston side pressure simulated and experimental.



Source: Author.

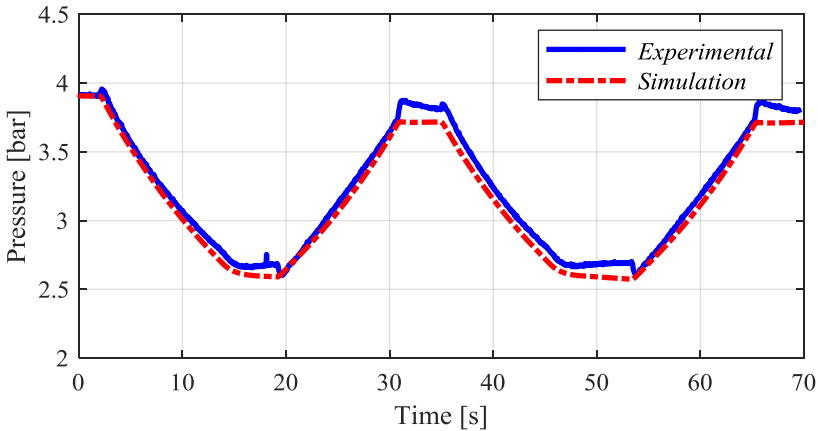
The same for Figure 5.8 and Figure 5.9 showing the pressure in the rod side chamber and in the accumulator line, respectively.

Figure 5.8 - Rod side pressure simulated and experimental.



Source: Author.

Figure 5.9 - Pressure in the accumulator line.



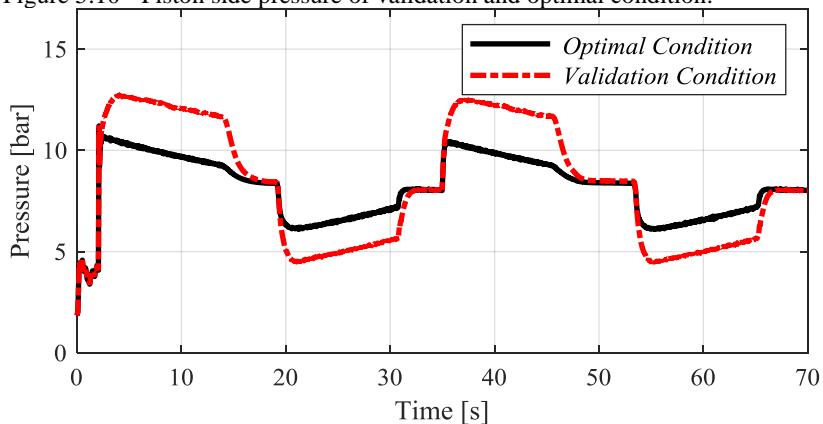
Source: Author.

Comparing both model and experiment data, the mathematical model was considered proper to reproduce the real behavior of the system analyzed. As the model is assumed validated, the next section presents the analysis of energies inside the system and determine the energy efficiency performance of the system.

As mentioned previously regarding the size of the pump/motor in the rod side chamber, after the model was validated, a test simulating the optimal condition of volumetric displacement ratio was done just to

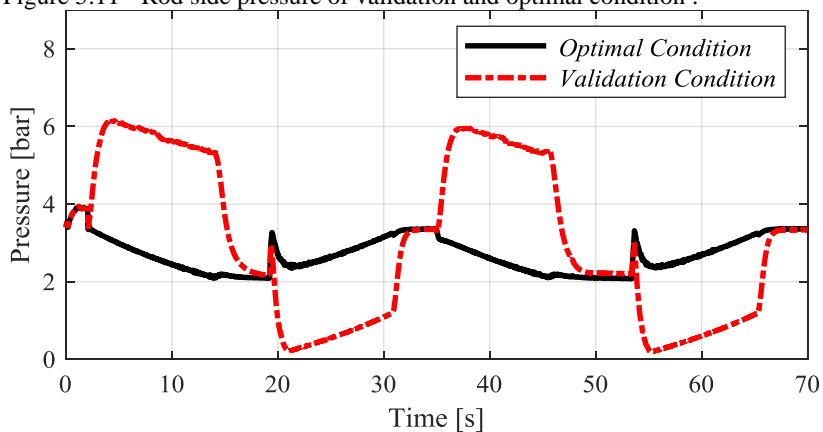
illustrate that there is a dynamic effect on the pressure when the electric motor is reversed, however it is not enough to decrease too much the pressure level. Figure 5.10, Figure 5.11 and Figure 5.12 present the level pressures of the system using the same conditions of the validation, changing just the volumetric displacement of the pump/motor B to the optimal value.

Figure 5.10 - Piston side pressure of validation and optimal condition.



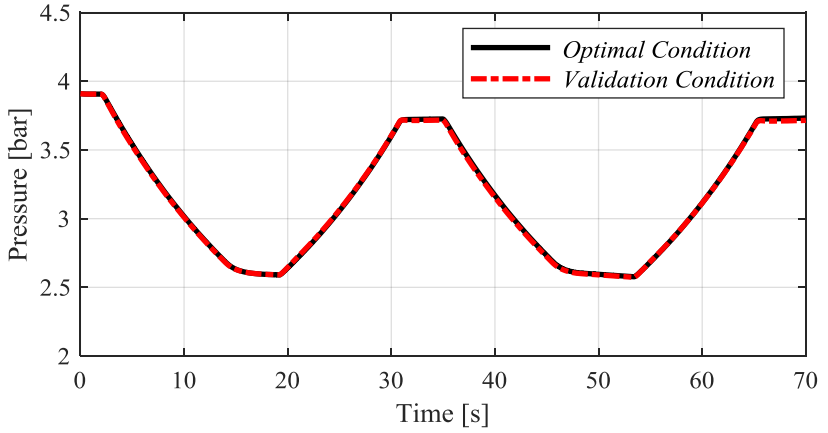
Source: Author.

Figure 5.11 - Rod side pressure of validation and optimal condition .



Source: Author.

Figure 5.12 - Pressure in the accumulator line of validation and optimal condition .



Source: Author.

6. ANALYSIS

In this section, the system is analyzed in terms of power and energy efficiency and regeneration during the performed cycle presented in the previous chapter. The equations used are presented and the discussion regarding the results obtained.

The power at the axis of the electric motor is defined as

$$P_{em} = T \cdot \omega, \quad (6.1)$$

where T is the total torque required by both pump/motors, calculated by Equation 4.12. The power of the electric motor is the input power to drive the pump/motors and it is converted into hydraulic power defined as

$$P_{hyd} = q \cdot \Delta p, \quad (6.2)$$

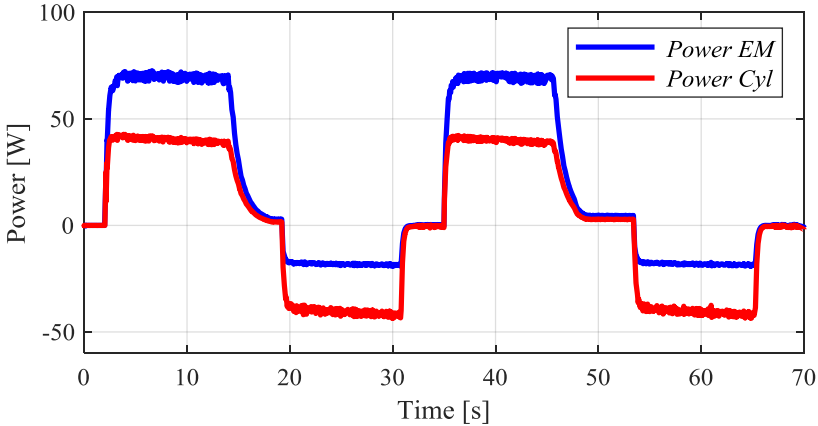
where q is the volumetric flow rate supplied by the pump/motor, and Δp the pressure over the pump/motor. The hydraulic power is transmitted to the actuator and transformed in useful power (or mechanical), which is described as

$$P_{cyl} = F_{cyl} \cdot \dot{x}, \quad (6.3)$$

where F_{cyl} is the force applied by the actuator and \dot{x} the cylinder velocity.

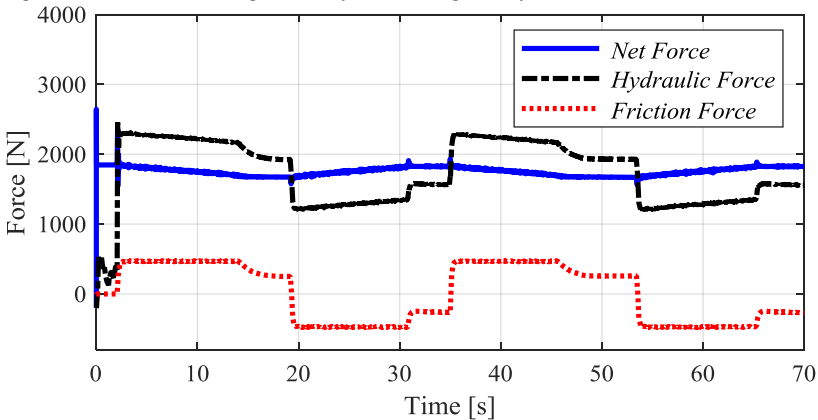
Figure 6.1 shows the instantaneous powers calculated by Equations 6.1, and 6.3 during the performed motion. Figure 6.2 shows the forces acting in the system to evaluate the effect of the friction in the actuator.

Figure 6.1- Power supplied and consumed during the cycle.



Source: Author.

Figure 6.2 - Forces acting in the system along the cycle.



Source: Author.

Analyzing Figure 6.1, when the cylinder is lifting (positive powers), the energy available to execute useful work is quite smaller than the power provided by the motor shaft. It is caused mainly by the friction force on the cylinder (22.38%), mechanical (22.24%) and volumetric losses (1.7%) in the pump/motor.

When the cylinder is lowering (negative power), there is an amount of potential energy stored in the load, in this case, it is considered the input power, and the power in the pump/motor shaft is

considered the output power. In this case, as the pump/motor is connected to the electric motor, the output power available can be regenerated. This part of the cycle has an important discussion regarding the output power present in this experiment. The losses in this lowering cycle are influenced by friction forces, pump leakage, and the torque at the electric motor. At this moment, the electric motor is not just setting the rotational frequency but also maintaining it, or in other words, is breaking the actuator velocity which also consumes energy.

Two scenarios can be observed for this system, the first one is that when the set electric motor - frequency converter has not an energy storage system or is not connected to the grid. Consequently, the potential energy is totally wasted. The second situation is when the system is connected to the grid or an energy storage device.

Assuming that the system is able to regenerate energy, the lowering motion is not wasting energy, so the efficiency along the whole cycle performed is calculated. The energies and efficiencies calculated indicate only hydraulic and mechanical. The energy required in the shaft and the energy regenerated available in the shaft when operating in generator mode is given by Equation 6.4.

$$E_{shaft} = \int T \cdot \omega \cdot dt, \quad (6.4)$$

In a similar way, the energy available in the cylinder is determined to integrate the power on it.

$$E_{cyl} = \int F_{cyl} \cdot \dot{x} \cdot dt. \quad (6.5)$$

During the cycle, it is necessary to calculate energy efficiency differently for each motion. When lifting, the electric motor provides energy to the system resulting in a gain of potential energy. On the other hand, when the cylinder is lowering, the energy from the cylinder should be seen as input energy and the motor the output. The input and output energy equations are shown below according to the motion performed.

$$E_{input} = \int_0^{t1} T \cdot \omega \cdot dt + \int_{t1}^{t2} F_{cyl} \cdot \dot{x} \cdot dt + \int_{t2}^{t3} T \cdot \omega \cdot dt + \int_{t3}^{t4} F_{cyl} \cdot \dot{x} \cdot dt, \quad (6.6)$$

And

$$E_{output} = \int_0^{t1} F_{Cyl} \cdot \dot{x} \cdot dt + \int_{t1}^{t2} T \cdot \omega \cdot dt + \int_{t2}^{t3} F_{Cyl} \cdot \dot{x} \cdot dt + \int_{t3}^{t4} T \cdot \omega \cdot dt. \quad (6.7)$$

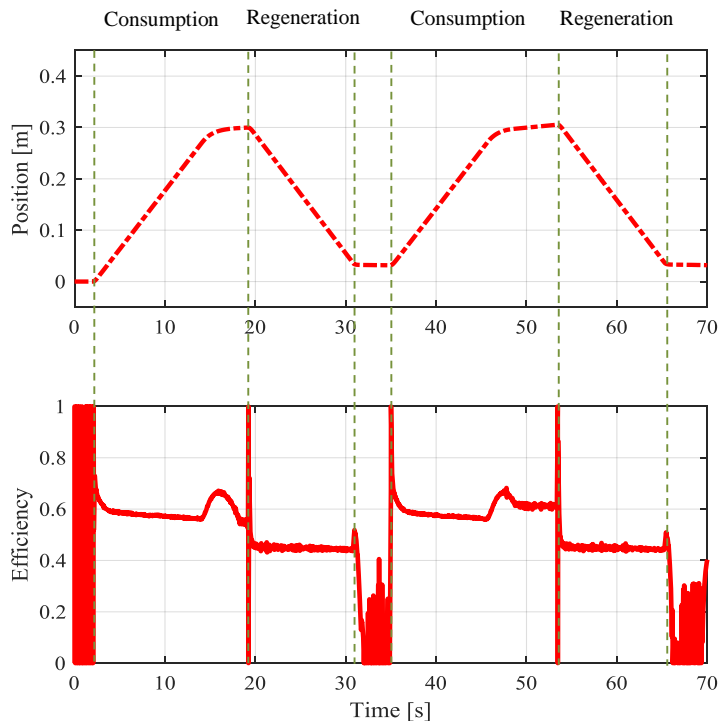
The total energy efficiency is determined by

$$\eta_{total} = \frac{E_{output}}{E_{input}}. \quad (6.8)$$

When the cycle is not considering the capacity of regeneration, the second and fourth terms of Equation 6.7 are null, due to the torque assumed zero, consequently the total efficiency decreases.

The instantaneous efficiency calculated by the simulation for the performed cycle is presented in Figure 6.3. The time periods from 2 to 19 seconds and from 35 to 54 seconds are representing the efficiency of the system during the lifting motion, when the curve goes to zero value it is neglected, when the regeneration mode starts operating. Analyzing the constant velocity period of the actuator displacement, the consumption efficiencies are between 56% to 66%, with some variations during slowdown and acceleration. For the lowering motion, the time periods from 19 to 31 seconds and from 54 to 65 seconds indicate the percentage of energy that is regenerated. The energy available to store or send it back to the grid is in a range of 45% to 46%. The transient part can be ignored, especially in the first seconds of simulation, once these behaviors are caused by initial values and numerical calculations related to pump leakages and initial position.

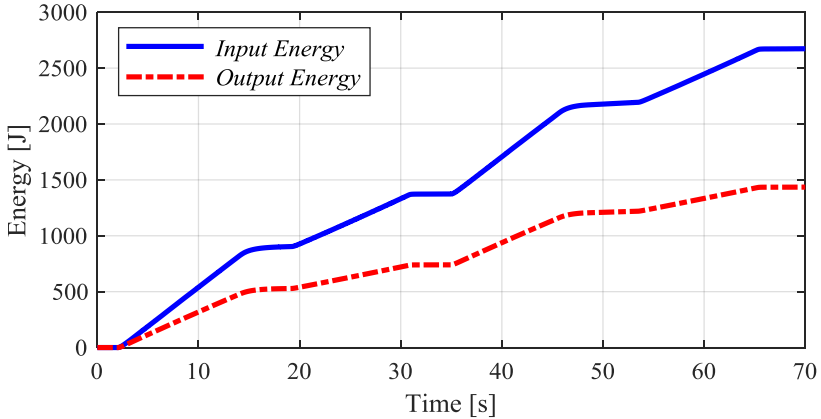
Figure 6.3 Efficiency results in the simulation.



Source: Author.

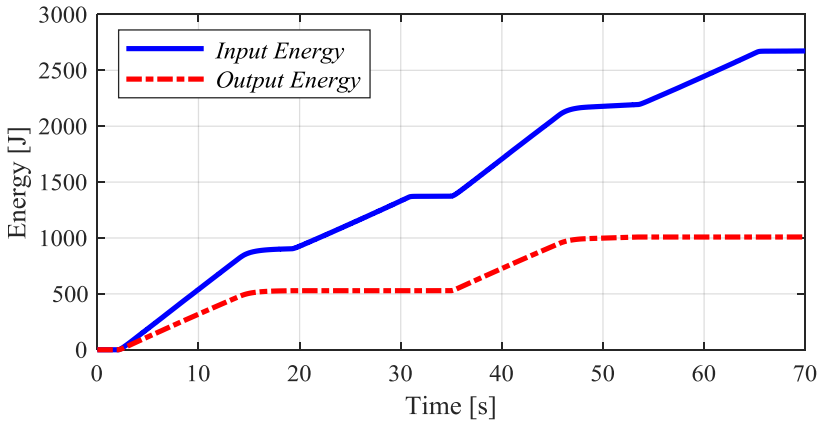
To have a general view of the cycle efficiency, the overall efficiency for the system during the whole motion (see the cycle in Figure 5.6) is calculated. It was determined using the input and output energies. The same manner, the efficiencies were estimated for lifting and lowering separately. Figure 6.4 shows the overall energy advancing and retreating the cylinder. In this case, is analyzed considering the capacity of regeneration. Figure 6.5 is the energy along the cycle considering the lowering motion the energy in the shaft is dissipated (no regeneration).

Figure 6.4 - Energy provided (solid line) and consumed (dashed line) during the cycle considering capacity of regeneration.



Source: Author.

Figure 6.5 - Energy provided (solid line) and consumed (dashed line) during the cycle considering no capacity of regeneration.



Source: Author.

The results obtained in this case were 53.68% of efficiency when considers the capacity of regeneration in the system. Without the capacity of regenerate energy, the output available in the pump/motor shaft is considered zero, resulting in a total efficiency of 37.74%.

In order to check if these values could be considered reasonable, another study published by the researches of the hydraulic group was utilized.

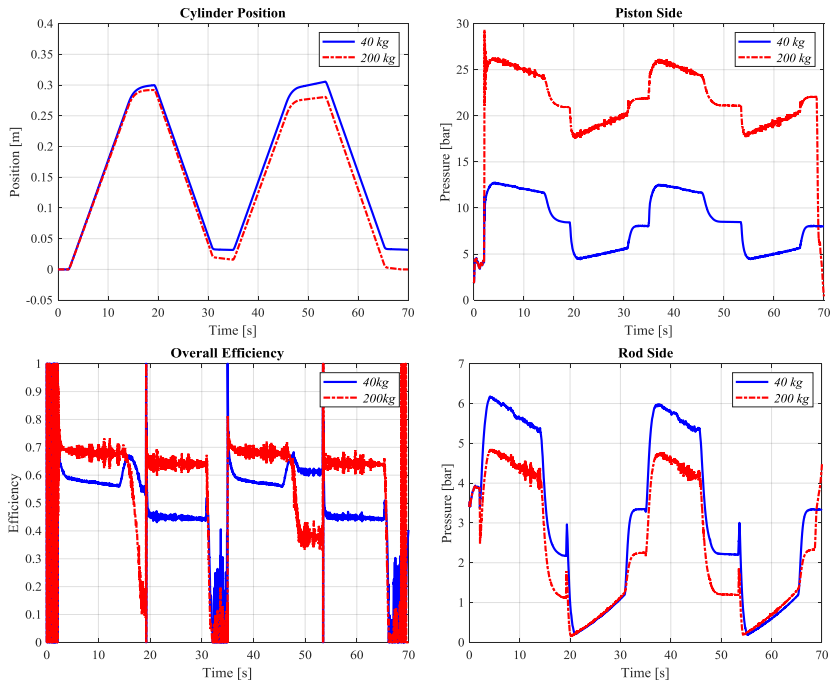
In Martinovski *et al* (2018), a similar drive concept was studied for a mining loader machine. The efficiencies observed were in a range of 44% - 60% depending on the load and velocities. Furthermore, the regeneration found in their work was in a range of 38% - 48%. These values take into account the electric motor and battery efficiencies.

Comparing the results obtained in this present work with the mentioned above, it is important to mention that the rotational speed set is considerably slower (12%) of the rated speed of the electric motor, it leads to a low electrical motor efficiency. It means that the faster the motion, the higher is the electrical efficiency can get. This is also valid for the pump/motor; the minimum speed specified by the manufacturer is between 600 rpm and 700 rpm. Low speed implies low volumetric efficiency and this effect is included in the model.

Secondly, the load utilized for testing can be considered smaller than it can handle. When looking at the pressure levels, the highest is about 13 bar in the piston chamber. The maximum pressure in the experiment corresponds to 6.8% of the maximum pressure allowed in the cylinder and 5.2% of the maximum pressure allowed by the pump/motors. Taking this into account, it is clear that the components are over-dimensioned in this case. A simulation was done to compare the efficiency utilizing the same input signal of the rotational speed electric motor but with load mass 5 times bigger (200 kg). The resulting efficiency to lift changed from 58% to 68% and the regeneration from 46% to 64%. It is important to mention that the cylinder did not reach the same range of motion, with losses up to 3 centimeters of height due to higher leakages in the pump/motor, but the bigger load increased the regeneration capacity significantly. The curves of the simulation are shown in Figure 6.6.

The pump/motor sizes have an important influence in the system performance. In this configuration, it is necessary to match the displacement according to the area of the actuator, the volumetric displacement ratio is about 0.7177 and area ratio is 0.75. Otherwise, one of the pump/motors will serve as a restriction also. However, it is unlikely that utilizing gear pump/motors the displacements will match, due to the variable leakage they present depending on the rotational speed, work pressure, and manufacturing differences.

Figure 6.6 - Simulation curves using 200 kg load compared with 40 kg



Source: Author.

In this experiment, even not knowing the exact displacement of the pump/motors, it was concluded that the rod side pump/motor is a bit smaller than it should be for this actuator. Looking at the pressures measurements, when the actuator lifts, the pressure on both sides are increasing, meaning that the pump/motor on the rod side is giving some restriction while pulling fluid out of the chamber (see Figure 5.8). On the other hand, when lowering, the pressure drops quickly depending on the rotational speed, because the volumetric displacement is not enough to compensate when the pump/motor on the piston head side is pulling fluid out (see Figure 5.11). Thinking of that, the check valves were installed to avoid the pressure drops too much, however, looking at the pressures on the rod side chamber and the accumulator line, the valve is opening when a pressure difference is 2.5 bar and the cracking pressure specified by the manufacturer is 0.5 bar. This fact is causing a very low-pressure level depending on the speed and time of the motion, and can cause cavitation. If the valves can open with 0.5 bar difference, the

pressure does not get too low and can operate safely without risk of cavitation.

Another analysis was done trying to find a better operation condition that could result in higher efficiency and regeneration level with this configuration. The rotational frequency becomes very limited depending on the relation between the volumetric displacement ratio of the pump/motors and the area ratio of the cylinder. The faster the actuator motion during lifting, the higher is the resistance of the pump/motor on the rod side, causing a back pressure that drastically reduces the efficiency. In order to calculate the efficiency of the system in a higher rotational (600 rpm), the volumetric displacement of pump/motor B need to be bigger (at least on simulation). The system is very sensible and the efficiencies are directly influenced by the load, cylinder velocity, and pump/motors displacement. A simulation with an input signal of 600 rpm, with 200 kg load mass and increasing the pump/motor B size was carried out to analyze the influence on the efficiency and regeneration levels. Table 6.1 shows the efficiency and regeneration values for different volumetric displacement values.

Table 6.1 - Influence of volumetric displacement ratio in the hydraulic efficiency and regeneration.

Volumetric displacement ratio (D_B/D_A)				
Ratio	0.7177	0.73	0.74	0.75
Overall efficiency				
With Regeneration	0.5477	0.5576	0.5745	0.6738
Without Regeneration	0.3426	0.3484	0.3588	0.4202

Source: Author.

The advantages with this system are that utilizing electric energy to provide power for the actuator, there is no dependency on the combustion engine during the duty cycle. Considering an excavator for instance, with three actuators being powered electrically, the size of the combustion engine can be reduced if battery power packs are available, consequently reducing consumption and emissions. The electro-hydrostatic concept also takes the advantages of the high efficiencies of the electric components, if operating in optimal conditions. The pump-controlled actuation drive has demonstrated in several studies its convenience, once the throttle losses are practically eliminated and use power on demand. The last, the capacity of regenerate energy from the

potential energy obtained after lifting, while in a conventional system when utilizing open reservoir the whole energy is wasted.

Besides all the positive aspects mentioned above, the system presents also disadvantages. Firstly, designing a closed system for an asymmetrical actuator has some challenges. To handle with different inlet and outlet flows in the cylinder requires precise dimensioning and selection of the components, otherwise, it can offer some limitations. As the idea was to build a system with the components commercially available, the area ratio and displacement ratio will hardly match. The main reason is the uncertainty found on the actual displacements and leakages in the components. The external gear working principle was considered due to its robustness and low cost. However, the volumetric displacements and leakages are unpredictable and an efficiency map should be taken experimentally to have more precise values. Another issue regarding the leakages is to maintain the cylinder position when the electric motor stops. The position cannot be kept and the motor would have to run in a very small rotational frequency to compensate the leak, consuming energy for no useful work. In addition, the number of components increases, consequently the costs since each actuator requires its own electric motor and pumps. The costs also consider the frequency converters and the battery pack needed to store and supply energy. Depending on the machine power, the limited space can have some restrictions related to the size and power of the battery pack. For now, this should be well studied considering just a small mobile machine.

The addition of more components also increase the weight of the machine, each unit composed of two pump/motors and one electric motor can reach up to 25 kg. Lastly, considering that is a closed-loop circuit, the continuous operation may cause detrition and the foulness should somehow be filtered to not damage even more the components.

7. CONCLUSIONS AND FUTURE WORKS

The concept of the electro-hydrostatic actuator using an asymmetrical cylinder was modeled and tested in a mobile crane. The mathematical model created in Matlab/Simulink was validated considering the convergence of the simulation curves with the experimental data, representing quite well the displacement and pressure behaviors.

With the model validated, an analysis of energy was carried out through the simulation results. It also allowed evaluating the system efficiency and behavior under different conditions of load and speed. For the condition tested in the test bench, efficiency reached up to 58 % during lifting and considering the capacity of regenerate, the efficiency of regeneration was observed about 46% during the lowering motion. The overall efficiency resulted in 54.77% in the cycle performed. The same condition was calculated however the capacity of regeneration was neglected, resulting in efficiency of 34.26%.

This configuration was designed to be a compact and closed-loop circuit unit in order to make the attachment easier and as close as possible of the actuator. Due to the closed-loop circuit configuration, the system presented a high sensibility on its behavior, especially because of the volumetric displacement of the pump/motors. If the volumetric displacement ratio is not matching the cylinder area ratio, there is a negative influence on the system efficiency caused by the counterforce generated. This was concluded comparing the efficiencies with different ratios, and the optimal volumetric displacement ratio has shown a substantial increase compared to ratios closed to optimal. The bigger the difference to the optimal ratio the slower the cylinder can be moved without opening the relief valves and check valves.

The efficiency is also influenced by the load submitted, when higher loads are applied, the friction portion of the losses is smaller comparing to the total force, on the other hand the volumetric losses in the pump/motors are higher. In this case, is due to the vertical position of the actuator handling with just compressive load. In addition, when the electric motor stops running it is possible to notice the cylinder retracting on its own, without the capacity to keep the position due to the internal leakage in the pump/motors.

The concept of electro-hydrostatic actuator for asymmetrical cylinder has shown promising benefits with respect to the efficiency. The mismatch between volumetric displacement ratio and area ratio will

be hardly avoided, however it can be overcome, with minor limitations, using mechanisms to compensate the mismatch.

7.1 FUTURE WORKS

With the conclusion and further analysis in this thesis, a few suggestions for future works are mentioned:

- Considering that this system concept is intended not just for stationary but especially mobile applications, such as excavator, it is necessary to evaluate the behavior of the system when submitted to dynamic loads and situations with sudden peak pressures. For example, in conditions of digging cycles when resistive forces act in the bucket cylinder. In addition, while the cycle I performed the force in a specific cylinder can quickly change from compressive load to tensile load;
- A position control system is necessary to perform the desired cycle. The pump/motors present leakages affecting the cylinder position when the electric motor is not operating. One possibility is the usage of on-off valves to keep the actuator position without the necessity of the electric motor run in small rotational speed, which consumes power just to compensate internal leakages;
- A thermal study should be carried out since the system has not worked for long periods and cycles, the heat exchange needs to be observed to check the necessity of water cooling system or if natural cooling is enough. The environment temperature also has an important role in the behavior of the system. The performance of the system is directly affected especially if working in harsh conditions such as winter time in northern Europe;
- Finally, it is proposed the evaluation of different configurations previously showed at the beginning of this thesis, for example utilizing just one pump/motor, two pump/motors and two electric motors, hydraulic transformers, digital pumps and so on.

BIBLIOGRAPHY

Alle, N. *et al.* Review on electro-hydrostatic actuator for flight control. *International Journal of Fluid Power*, 2016, 17.2: 125-145.

Armstrong, B.; Canudas-de-Wit, C. Friction modeling and compensation. In: *The control handbook*. CRC Press, 1996. P .1369-1382. Cap. 77.

Bacca, G. A., De Negri, V. J., Assaf, Y. Modelo Matemático No-Linear para un Servosistema Neumático de Posicionamento Preciso. *Revista Tecnológicas* No.24, Julio de 2010.

Belan, H. C., Locateli, C. C., Lantto B., Krus, P., De Negri, J. V. Digital Secondary Control Architecture For Aircraft Application. *The Seventh Workshop on Digital Fluid Power*, February 26–27, 2015, Linz, Austria

Belan, H. C., Fallgatter, R., Bregalda, R., De Negri, V. J. Técnicas De Dimensionamento E Implementação Para Um Sistema Hidráulico Digital. *Congresso Nacional de Engenharia Mecânica- CONEM*, Fortaleza, Ceará. 21-25 de Agosto, 2016.

Bonchis, A., Corke, P. i., Rye, D. C. A Pressure-Based, Velocity Independent, Friction Model for Asymmetric Hydraulic Cylinders. *Robotics and Automation*, 1999. *Proceedings. 1999 IEEE International Conference on: IEEE*. 3: 1746-1751 p.1999.

Cho, Baek-Hyun; Lee, Hyoun-Woo; Oh, Jong-Sun. Estimation technique of air content in automatic transmission fluid by measuring effective bulk modulus. *Int. J. Automot. Technol*, v. 3, n. 2, p. 57-61, 2002

Costa, G. K.; Sepehri, N. *Hydrostatic Transmissions and Actuators: Operation, Modelling and Applications*. Wiley, 2015.

Dahmann, P. Closed Loop and Position Control of a Hydraulic Manipulator in Brick Works with a Frequency Controlled Internal Gear Pump in Motor/Pump Operation, 3rd International Fluid Power Conference. Aachen, Germany, 2002.

Dalla Lana, E. Avaliação do rendimento de bombas hidráulicas de engrenagens externas através de medição de temperatura. 2005. 100 p. Dissertação (Mestrado em Engenharia Mecânica). Universidade Federal de Santa Catarina, Florianópolis.

Dalla Lana, E., De Negri, V. J. A New Evaluation Method for Hydraulic Gear Pump Efficiency through Temperature Measurements. In: SAE 2006 Commercial Vehicle Engineering Congress and Exhibition. Chicago – USA, 31 de Outubro a 02 de Novembro de 2006.

Destro, M. Análise de condições operacionais críticas em posicionadores eletro-hidráulicos. 2014. 138 p. Dissertação (Mestrado em Engenharia Mecânica). Universidade Federal de Santa Catarina, Florianópolis.

Dupont, P. E. The Effect of Friction on the Forward Dynamics Problem. *International Journal of Robotics Research*, 12(2): 164-179, April 1993.

Destro M. & De Negri, V. Method for combining valves with symmetric and asymmetric cylinders for hydraulic systems, *International Journal of Fluid Power*, 19:3, 126-139, 2018 DOI: 10.1080/14399776.2018.1483164

Ellman, A., Piché, R. Modified Orifice Flow Formula for Numerical Simulation of Fluid Power Systems. *ASME Fluid Power System and Technology: Collected Papers*, 1996.

Gaile, A.; Reard, Y. Electro Hydraulic Actuation (EHA) systems for primary flight control, Landing gear and other type of actuation. In: *Aircraft Utility Systems (AUS)*, IEEE International Conference on. IEEE, 2016 p. 723-728.

Gholizadeh, H., Bitner, D., Burton, R., & Schoenau, G. Modeling and experimental validation of the effective bulk modulus of a mixture of hydraulic oil and air. *Journal of Dynamic Systems, Measurement, and Control*, v. 136, n. 5, p. 051013, 2014.

Habibi, S.; Goldenberg A. Design of a New High Performance Electrohydraulic Actuator. *Advanced Intelligent Mechatronics*, 1999. *Proceedings, 1999 IEEE/ASME International Conference on*, 1999: 227~232.

Heitzig, S.; Theissen, H. 2011. "Aspects of digital pumps in closed circuit." *The Second Workshop on Digital Fluid Power*, 12-13 November 2011, Linz, Austria.

Helbig, A. Injection Moulding Machine with Electric-Hydrostatic Drives, 3rd International Fluid Power Conference, Aachen, Germany, 2002.

Hippalgaonkar, R.; Ivantysynova, M. A Series-Parallel Hybrid Mini-Excavator with Displacement Controlled Actuators. The Thirteenth Scandinavian International Conference on Fluid Power, Linköping, Sweden. 2013.

Järf, A. Flow Compensation Using Hydraulic Accumulator in Direct Driven Hydraulic Differential Cylinder Application and Effects on Energy Efficiency. Master's Thesis, Aalto University, Espoo, Finland, 2016.

Jiang, J. H.; Su, W. H.; Liu, Q. H. Direct Drive Variable Speed Electrohydraulic Servo System for Position Control of a Ship Rudder. 4th IFK, Dresden, Germany; 2004, pp. 103–114.

Kagoshima, M.; Komiyama, M.; Nanjo, T.; and Tsutsui, A. Development of New Hybrid Excavator. *Kobelco Technology Review*, (27): 39-42, 2007.

Kajaste, J.; Kauranne, H.; Ellman, A.; Pietola, M. Computational Models for Effective Bulk Modulus of Hydraulic Fluid. The Second International Conference on Computational Methods in Fluid Power, FPNI'06, Aalborg, Denmark, August 2-3, 2006. 2006. p. 7.

Komsta, J. Variable Speed Pump Drives for Industrial Machinery – System Considerations. *Fluid Power Systems Conference 2013*.

Linjama, M. *et al.*, 2009, "Secondary controlled multi-chamber hydraulic cylinder". The 11th Scandinavian International Conference on Fluid Power SICFP'09, Linköping, Sweden, 2009.

Linjama, M. Digital fluid power-state of the art. The Twelfth Scandinavian International Conference on Fluid Power, Tampere, Finland. 2011.

Linsingen, I. von. Fundamentos de Sistemas Hidráulicos. 5. Ed. rev.- Florianópolis: Ed. da UFSC 2016. 398p. il.- (Coleção Didática).

Lovrec, D. and Ulaga, S. Pressure Control in Hydraulic Systems With Variable or Constant Pumps. In: *Experimental Techniques*, Vol. 31, No. 2, pp. 33--41, 2007.

Manring, N. Hydraulic Control Systems. John Wiley & Sons, New Jersey, 2005. ISBN 0-471-69311-1.

Manring, N. D. Mapping the efficiency for a hydrostatic transmission. *Journal of Dynamic Systems, Measurement, and Control*, v. 138, n. 3, p. 031004, 2016.

Maré, J. C. Aerospace Actuators 2: Signal-by-wire and Power-by-wire. John Wiley & Sons, 2017.

Martinovski, T., Sourandes, T., Turunen, A., Minav T. & Pietola M. Control Strategy for a Direct Driven Hydraulics System in the Case of a Mining Loader. 11th International Fluid Power Conference (11. IFK), Aachen, Germany, pp.294-305, March 19-21, 2018

McCoy, D., Martin, H. R. Control of Fluid Power. Analysis and Design. 2.ed. England: Ellis Horwood Ltd., 1980.

McCullough, K. R. Design and Characterization of a Dual Electro-Hydrostatic Actuator. Master Thesis. McMaster University, Faculty of Engineering, Hamilton, Canada, January 2011.

Michel S, Weber J. Energy-efficient electrohydraulic compact drives for low power applications. In Bath Symposium on Power Transmission & Motion Control 2012 Sep.

Minav, T. Electric-Drive-Based Control and Electric Energy Regeneration in a Hydraulic System. Doctoral Dissertation. Lappeenranta University of Technology, Faculty of Technology, Electrical Engineering, Electrical Drives Technology, August 2011.

Quan, Z.; Quan L.; Zhang, J. Review of Energy Efficient Direct Pump Controlled Cylinder Electro-hydraulic Technology. *Renewable and Sustainable Energy Reviews* 35 (2014), 336-346.

Rabie, M. G. *Fluid Power Engineering*. New York: McGraw-Hill, 2009.
Stringer, J. D. *Hydraulic systems analysis*. 1976.

Taşner T., Les K., Tie V., Lovrec D. Energy Efficiency of Different Electro-hydraulic Drives. 9th International Fluid Power Conference (9. IFK), Aachen, Germany, pp.14-25, March 24-26, 2014.

Taşner, T. and Lovrec, D. Comparison of Modern Electrohydraulic Systems. In: *34th International Conference on Production Engineering*, Niš, pp. 253-256, 2011.

Teixeira, P. L. Análise Teórica Experimental de Prensa Dobradeira Hidráulica Controlada por Bomba-motor com Velocidade Variável. Dissertação de Mestrado. Universidade Federal de Santa Catarina, Florianópolis, Brasil, 2015.

Totten, G. E.; De Negri, V. J. *Handbook of Hydraulic Fluid Technology*. CRC Press, 2011. p.1-52. Chapter 1.

Tran, X. B.; Hafizah, N.; Yanada, H. Modeling of dynamic friction behaviors of hydraulic cylinders. *Mechatronics*, v. 22, n. 1, p. 65-75, 2012. ISSN 09574158.

Valdiero, A. C. Controle de Robôs Hidráulicos com compensação de atrito. 2005. 157 p. p. Tese (Programa de Pós-graduação em Engenharia Mecânica), Universidade Federal de Santa Catarina, Florianópolis.

Williamson, C.; Zimmerman, J.; Ivantysynova, J. Efficiency Study of an Excavator Hydraulic System Based on Displacement-Controlled Actuators. Bath ASME Symposium on Fluid Power and Motion Control- FMPC 2008 pp.297-307.

Xu, M., Jin, B., Chen, G., & Ni, J. (2013). Speed-control of energy regulation based variable-speed electrohydraulic drive. *Strojniški vestnik-Journal of Mechanical Engineering*, 59(7-8), 433-442.

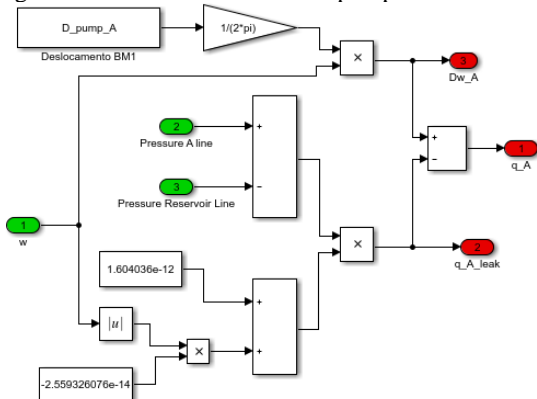
Zhang, J.; Chao, Q.; Xu, B. Analysis of The Cylinder Block Tilting Inertia Moment and Its Effect on The Performance of High-Speed Electro-Hydrostatic Actuator Pumps of Aircraft. *Chinese Journal of Aeronautics*, 2017a.

Zhang, S.; Minav, T.; Pietola, M. Decentralized Hydraulics for Micro Excavator. *The Fifteenth Scandinavian International Conference on Fluid Power*, Linköping, Sweden. 2017b.

Zhao, X.; Vacca, A. Formulation and Optimization of Involute Spur Gear in External Gear Pump. *Mechanism and Machine Theory*, v. 117, p. 114-132, 2017.

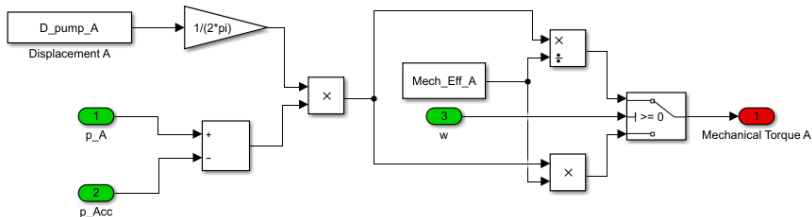
APPENDIX A - MATHEMATICAL MODEL OF THE ELECTRO-HYDROSTATIC ACTUATOR

Figure A.1- Volumetric flow rate pump/motor A



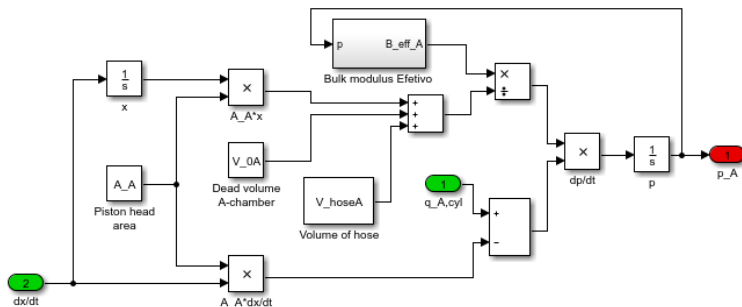
Source: Author.

Figure A.2 - Mechanical torque pump/motor A.



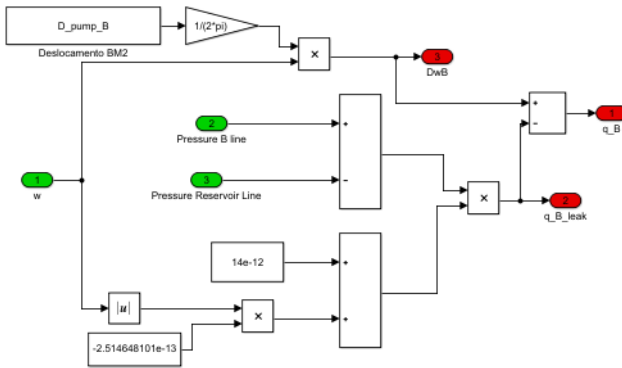
Source: Author

Figure A.3 - Pressure in the chamber A of the Cylinder.



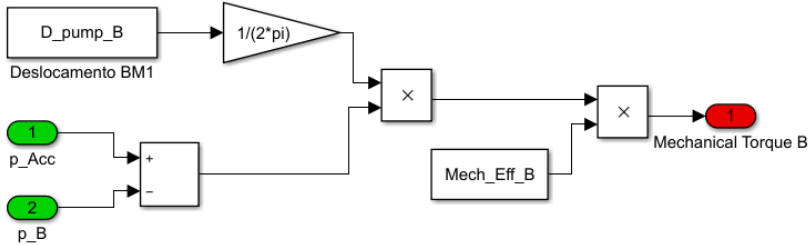
Source: Author

Figure A.4 - Volumetric flow rate pump/motor B.



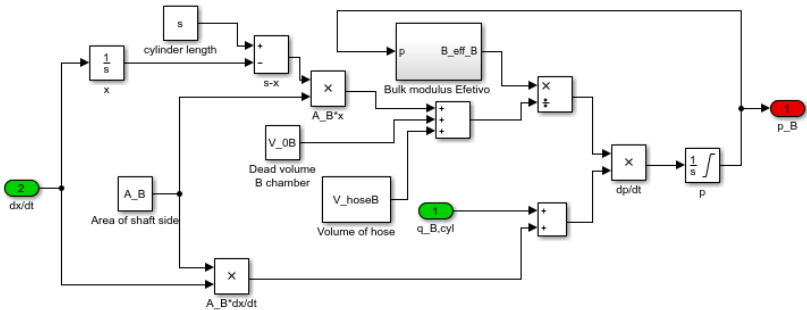
Source: Author.

Figure A.5 - Mechanical torque pump/motor B.



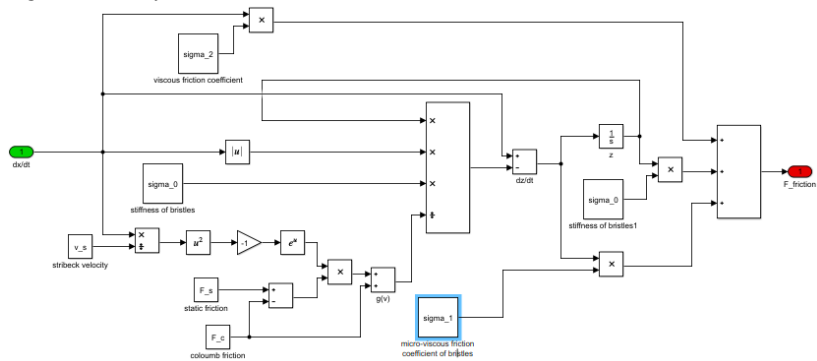
Source: Author.

Figure A.6 - Pressure in the chamber B of the cylinder.



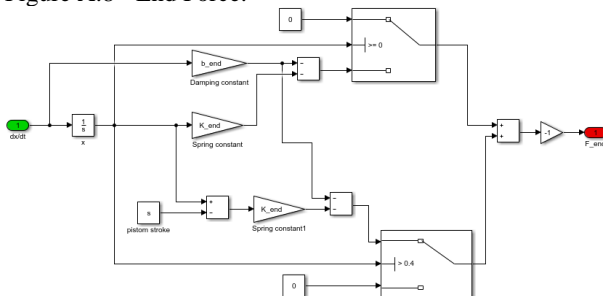
Source: Author.

Figure A.7 - Cylinder friction model.



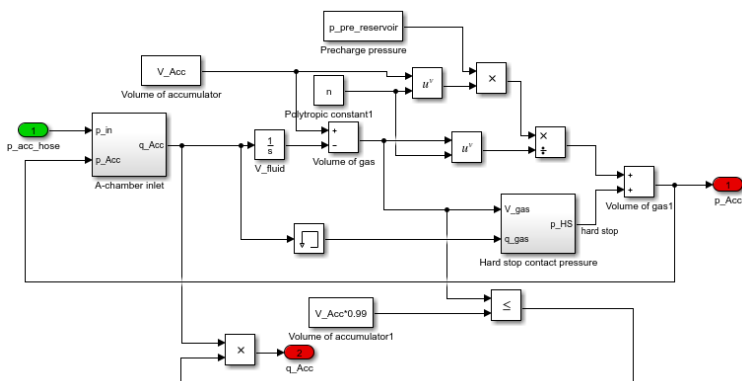
Source: Adapted from Jarf (2016).

Figure A.8 - End Force.



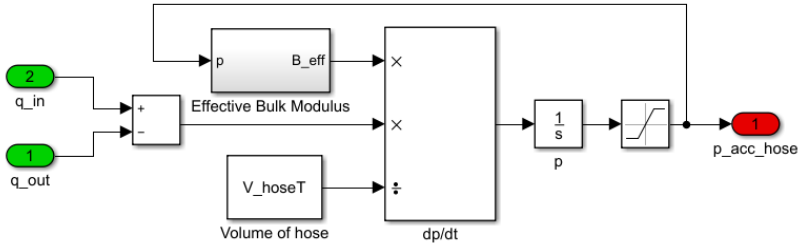
Source: Adapted from Jarf (2016).

Figure A.9 - Accumulator model.



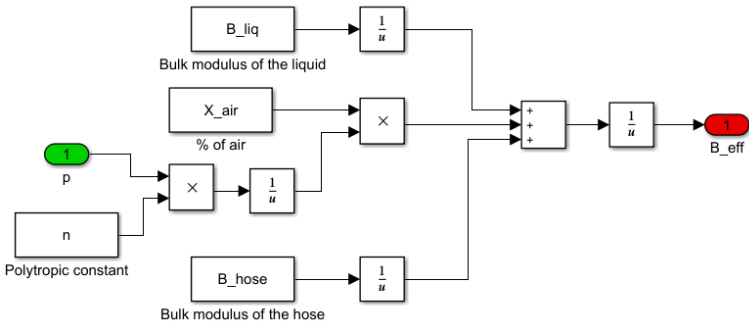
Source: Adapted from Jarf (2016).

Figure A.10 - Accumulator hose volume.



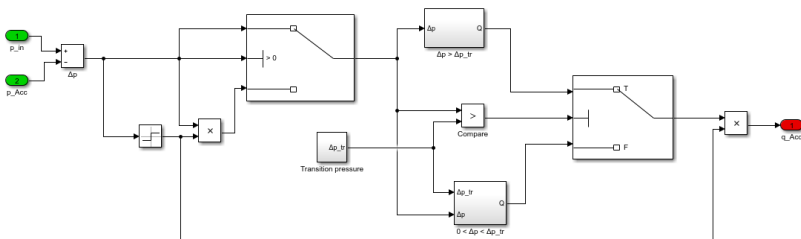
Source: Author.

Figure A.11 - Effective bulk modulus.



Source: Author

Figure A.12 - Orifice of the accumulator.



Source: Adapted from Jarf (2016).


```

rho = 860; % Density of fluid
[kg/m^3]

%% Bulk modulus model
n = 1.4; % Polytropic constant
X_air = 0.15/100; % Gas content of oil (free air)
B_liq = 1.4e9; % Bulk modulus of liquid
[litterature]
B_hose = 7e8; % Bulk Modulus of
flexible hose [litterature]

%% Cylinder specific parameters

d1 = 60/1000; % Piston diameter
[m]
d3 = 30/1000; % Piston shaft
diameter [m]
s = 0.4; % Piston stroke [m]

% Cylinder chamber
A_A = (pi/4)*d1^2; % A-side area
A_B = (pi/4)*(d1^2-d3^2); % B-side area
x_0 = 0; % Initial position
of piston
V_0A = 55.8e-6; % Dead volume, A-
side [m^3][Measured]
V_0B = 18.2e-6; % Dead volume, B-
side [m^3][measured]

% Accumulator Inlet
d_oAcc = 12/1000; % Accumulator inlet
diameter [measured]
A_oAcc = (pi/4)*d_oAcc^2; % Accumulator inlet
area [calculated]
C_qturb = 0.611; % Discharge
coefficient
Re_tr = 1000; % Critical reynolds
number
Nu = 30*1e-6; % Kinematic viscosity

```

```

% Friction model
F_c = 240.607; % Coloumb friction
[N] [Measured] 87.607
F_s = 300; % Static friction
[Measured] 300
v_s = 0.0005; % Stribeck velocity
[Measured] 0.0005
sigma_0 = F_s/0.001; % Stiffness constant
[estimated]
sigma_1 = sqrt(sigma_0); % Micro-viscous friction
coefficient [estimated]
sigma_2 = 10000; % Viscous friction
coefficient [Estimated]

% End force cylinder
K_end = 1e12 ; % Spring end force constant
A_A*120e5/0.2e-3
b_end = 1.5e7 ; % Damping end force constant
0.5*sqrt(K_end*m)

%% Pump/Motors

D_pump_A = 13.03e-6; %Volumetric displacement
pump/motor B [m^3/rev]
D_pump_B = 9.3512e-6; %Volumetric displacement
pump/motor B [m^3/rev]

Mech_Eff_A = 0.7456;
Mech_Eff_B = 0.7690;
Electric_Eff = 0.50;

%% Hoses

Beta = 1.4e9; %Módulo de Compressibilidade [Pa]

% Hose between A-pump and A-chamber
d_hoseA = 10/1000; % Diameter of hose
[measured]
l_hoseA = 1; % Length of hose
[measured]

```

```

V_hoseA = (pi/4)*d_hoseA^2*l_hoseA;      % Volume of
hose

% Hose between B-pump and B-chamber
d_hoseB = 8/1000;                        % Diameter of hose
[measured]
l_hoseB = 1.42;                          % Length of hose
[measured] 1.42
V_hoseB = (pi/4)*d_hoseB^2*l_hoseB;% Volume of hose

% Hose Tank Line
d_hoseT = 10/1000;                       % Diameter of hose
[measured]
l_hoseT = 2.14;                          % Length of hose
[measured]
V_hoseT = (pi/4)*d_hoseT^2*l_hoseT;      % Volume of
hose

p_init_PS = 1.85e5;                       % Initial Pressure
Piston Side Hose 2.5e5
p_init_RS = 3.4e5;                       % Initial Pressure Rod
Side Hose 3.42e5
p_init_T = 3.91e5;                       % Initial Reservoir
Pressure Hose

%% Accumulator

p_pre = 2e5;                              % Precharge pressure
[bar -> Pa]
p_pre_reservoir = 2e5;                   % Precharge pressure
reservoir [bar -> Pa]
V_Acc = 0.7/1000;                         % Total accumulator
volume [l -> m^3]

K_s = 5e10 ;                             % Hard-stop
stiffness coeff. [Pa/m^3] (litterature)
K_d = 0e9;                                % Hard-stop damping
coeff. [Pa*s/m^6] (litterature)
V_dead_Acc = 0.1*V_Acc;                  % Accumulator dead
volume (estimated)

```

```

p_atm = 1e5; % Atmospheric
pressure [bar]

%% Load

% Distance elements
r_c = 647.026/1000; % Distance to
cylinder upper fastening [cm->m]
r_m = 1674.05/1000; % Distance to mass
[cm->m]
r_1 = 693.744/1000; % Distance to first
segment centre of mass [mm->m]
r_2 = 977.217/1000; % Distance to
second segment centre of mass [mm->m]
r_cf = 98.3/100; % Distance to
cylinder rotation origin [cm->m]

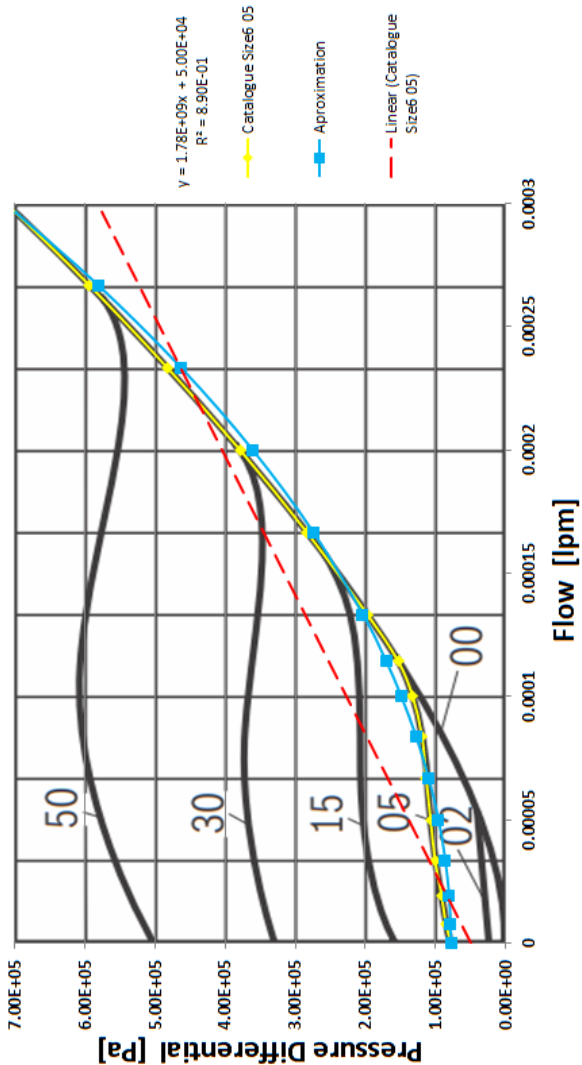
% Mass elements
m_r1 = 25.116192; % Mass at first segment
m_r2 = 21.3942; % Mass at second segment
J = m*r_m^2+m_r1*r_1^2+m_r2*r_2^2; % Simplified
moment of inertia for crane

theta_0 = 80; % Angle of boom when
cylinder fully retracted
theta_max = 115;
theta_1 = 0.1169; % [calculated]
theta_2 = 0.1572; % [calculated]
theta_load = 0.1775; % [calculated]

```


APPENDIX B- CURVE PRESSURE X FLOW OF CHECK VALVE FOR PARAMETER ESTIMATION

Figure B.1 - Curve Flow x Pressure of check valve.



Source: Author.